TECHNICAL NOTE

D-765

EXPERIMENTAL HEAT TRANSFER AND PRESSURE DROP OF LIQUID HYDROGEN FLOWING THROUGH A HEATED TUBE

By R. C. Hendricks, R. W. Graham, Y. Y. Hsu, and R. Friedman

Lewis Research Center
Cleveland, Ohio

NATIONAL AERONAUTICS AND SPACE ADMINISTRATION
WASHINGTON
May 1961

NATIONAL AERONAUTICS AND SPACE ADMINISTRATION

TECHNICAL NOTE D-765

EXPERIMENTAL HEAT TRANSFER AND PRESSURE DROP OF LIQUID HYDROGEN FLOWING THROUGH A HEATED TUBE

By R. C. Hendricks, R. W. Graham,
Y. Y. Hsu, and R. Friedman

SUMMARY

The heat-transfer and pressure-drop characteristics of liquid *para*-hydrogen flowing through a heated vertical tube were investigated over the following range of conditions: inlet pressure, 30 to 70 pounds per square inch; average heat flux, 1 Btu per square inch per second maximum; and temperature differential, 50° to 750° R between the fluid and the wall. As stored in the Dewar, the hydrogen was approximately 95 percent *para*. Two different test-section geometries of 1-foot length were employed; one had a 0.625-inch outside diameter and 0.065-inch wall, and the other a 0.375-inch outside diameter and 0.031-inch wall.

Local pressure drop and heat-transfer coefficients for boiling hydrogen are presented. The wall temperature profile along the tube was radically different from that observed in convective heat transfer with single-phase fluids. For the larger heat fluxes, a minimum wall temperature occurred somewhere near the end of the tube, and the maximum temperature occurred near the entrance. A vapor binding or dry-wall condition was apparent in some of the hydrogen runs. An empirical correlation for predicting the two-phase heat-transfer coefficient is presented.

Pressure-drop measurements showed that the frictional loss is small compared with the momentum loss. In fact, a one-dimensional momentum analysis can predict the pressure drop quite accurately.

INTRODUCTION

Liquid hydrogen appears to be a very attractive propellant either in chemical systems in which it is burned with an oxidant, or in monopropellant systems in which it is heated by some device like a nuclear reactor. Its low atomic weight, high specific heat, and high heat of combustion all contribute to high specific-impulse values for either of these types of propulsion systems. The undesirable characteristics of

the propellant include a large specific volume and the difficult handling procedures associated with a low-temperature cryogen.

Beyond the attractive propulsive qualities, hydrogen appears as a good coolant with an appreciable heat-sink capability. Since many components of a propulsion system must be cooled, this is a further argument for hydrogen as a propellant.

To evaluate liquid hydrogen properly as a coolant, more experimental information is required concerning the heat-transport mechanism for both subcritical and supercritical conditions. The problem is particularly acute for hydrogen, because it is generally used at conditions where density changes rapidly. For this report, subcritical pressures from 30 to 70 pounds per square inch absolute and a narrow range of bulk temperatures (low subcooling) are included in the experimental conditions. The heat-transfer characteristics of hydrogen were measured in an electrically heated vertical tube. The tube was instrumented for surface temperature and pressure-drop measurements. The temperature difference between the wall and bulk was varied from approximately 50° to 750° R. The maximum heat flux was 1 Btu per square inch per second.

For the range of investigation, film boiling of the hydrogen and a resulting two-phase flow phenomenon occurred. The heat-transfer and pressure-drop results are discussed in terms of a two-phase flow model. A correlation scheme is presented that is similar to methods employed in correlating two-phase heat-transfer processes with other fluids.

One of the variables employed in the heat-transfer correlation is the Martinelli two-phase parameter X_{tt}, which is an index of wall and two-phase shear resistance of the two-phase flow. Originally presented in reference 1, this parameter was used to predict two-phase pressure drop from an estimate of the gas-phase pressure drop. Martinelli's friction correlation was applied to a gaseous core and a liquid annulus flowing isothermally in a pipe. Appendix D shows that the same two-phase parameter X_{tt} evolves from an analysis similar to Martinelli's for a liquid core and a gaseous annulus. Consequently, the application of this parameter to the hydrogen two-phase flow is justified.

Several researchers including Guerrieri and Talty (ref. 2) and Dengler and Addoms (ref. 3) have correlated two-phase fluid heat transfer using the Martinelli parameter. A similar empirical approach is applied to the film-boiling data of liquid hydrogen reported herein.

APPARATUS

Flow System

The test installation is shown schematically in figure 1. Liquid hydrogen, stored in a large Dewar, was forced through the flow system by external gaseous hydrogen pressure. The entrance piping to the test section and the test section itself were vacuum-jacketed to minimize heat leakage. After passing through the test section, the hydrogen entered a steam heat exchanger where it was completely vaporized, metered, and then exhausted into the atmosphere. All elements of the stack discharge system were thoroughly grounded to prevent buildup of static electrical charge.

Flow rate and pressure level were controlled by remotely operated valves upstream and downstream of the test section.

Test Section

A sketch of the vertical-tube heat-transfer test section is shown in figure 2. Two test-section geometries were used; the first was a stainless-steel tube of 0.625-inch outside diameter and 0.065-inch wall, and the second was an Inconel tube of 0.375-inch outside diameter and 0.031-inch wall. The heated portions of both geometries were 12 inches long. Approximately 5 inches of unheated test section preceded the heated portion. The smaller Inconel tube was more extensively instrumented for local pressure measurements. Because of the importance of pressure data in determining local heat-transfer conditions, the overall data from the smaller tube were more amenable to analysis. The test section was electrically heated by the secondary of a 65-kilovolt-ampere alternating-current power supply (fig. 1). The maximum rated output of the secondary was 13 volts at 5000 amperes. The test section was electrically insulated from the adjacent piping of the flow apparatus by thin Teflon gaskets and insulating grommets in the flange connections.

Instrumentation

The measuring stations and types of measurement used for the 0.375-inch Inconel tube are shown schematically in figure 2. The hydrogen flow rate was metered upstream of the test section by a Venturi and downstream of the heat exchanger by an orifice. The two flowmeters served as checks on each other.

The test sections were instrumented with copper-constantan thermocouples silver-soldered to the outside wall. Additional thermocouples

were placed on the copper flanges to check heat leakage from the test section. All thermocouples employed an atmospheric boiling nitrogen cold junction.

Pressure taps were located upstream and downstream of the test sections and along the heated portion of only the Inconel tube.

PROCEDURE

Operating Conditions

The following ranges of operating conditions were investigated: flow rate, from 0.03 to 0.19 pound-mass per second; inlet pressure, from 30 to 70 pounds per square inch absolute; and electrical power input, from 0 to 14 Btu per second.

Data Recording

During a run, pressure, flow rate, temperature, and electrical power were recorded on tape by an automatic voltage digitizer (ref. 4) and were available for immediate write-back on an electric typewriter. The data tapes were processed by a high-speed computer, which converted the data bits into the desired parameters for further analysis. Periodic checks of the digitized recording were made on conventional self-balancing potentiometers and on a multichannel oscillograph.

Analysis of Data

Symbols are listed in appendix A, and equations and assumptions employed in reducing the experimental data appear in appendix B. The reader should become acquainted with appendix B as reference is made to definitions and equations therein throughout the DISCUSSION OF RESULTS.

The analysis of the heat losses peculiar to the apparatus is also presented in appendix B. It is sufficient to say here that the heat leakage into or out of the test section was negligible. The table in appendix B is included for the reader who may be interested in actual numerical values of the heat loss.

The thermodynamic and transport data of gaseous and liquid hydrogen used in the computation of results are presented as the last figures herein, numbered 8(a) to (f). These data are reproduced herein because they are compiled from several sources, some published (refs. 5 to 9) and some unpublished. Also, since there are insufficient experimental property and transport data at the present time, the authors extrapolated these data for their own use. For example, the only reliable viscosity

and specific-heat data for liquid hydrogen pertain to 1-atmosphere pressure, but the data were applied to conditions at several atmospheres. As more reliable data become available, the reader may apply correction ratios to these results to obtain results consistent with the new data.

DISCUSSION OF RESULTS

The experimental data and some selected results for the 0.375-inch-outside-diameter Inconel tube are tabulated in table I.

Wall Temperature Profiles

Figure 3(a) is a family of inside-wall temperature profiles for various flow rates and heat fluxes. These represent typical tube temperature profiles from the 0.375-inch Inconel tube, which are similar in characteristics to those obtained with the 0.625-inch stainless-steel tube (fig. 3(b)). At the lower heat fluxes, the profile is rather flat; but, as the heat flux is increased, the temperature profile takes on a negative slope. Opposite to single-phase heat-transfer results, the tube wall is actually hotter at the entrance than at the exit.

At first, it was thought that para to ortho conversion at the tube wall might be influencing the tube temperature profile. However, an analysis of the conversion reaction, as presented in appendix C, led to the conclusion that no appreciable endothermic reaction could occur in the vicinity of the tube wall, even though the wall material was catalytic; the conversion rate is negligibly low. To verify this conclusion, the interior of the stainless-steel test section was brush-plated with gold. Within the experimental accuracy, no differences in temperature were observed.

A more reasonable explanation for the wall temperature profile can be developed by considering a simple one-dimensional model of the flow. As the hydrogen enters the test section, immediately a thin vapor film is established adjacent to the wall. When saturation conditions are reached, a more turbulent exchange between the nonstable vapor film and the liquid core takes place. While this exchange mechanism probably represents a nonequilibrium condition because gas is generated at the wall and also in the liquid core as pressure is reduced, equilibrium conditions were assumed in evaluating quality. As the mixture moves through the heated tube, more gas is generated, and continuity considerations demand that the mixture velocity increase, which decreases the pressure. A pressure decrease, lowering saturation level, requires the fluid to absorb a portion of the latent heat, thereby decreasing density and increasing velocity. As in any turbulent convective heat-transfer process, increasing the velocity enhances the heat-transfer mechanism; consequently, the wall temperature drops. The vapor generated before saturation is assumed small and is a good approximation for small

subcooling; however, for large subcooling, the vapor generated must be considered (see appendix B).

There are two important exceptions to the condition where the tube temperature diminished monotonically from the inlet to the exit of the test section. For the first exception, the liquid hydrogen entered the test section subcooled and consequently did not reach saturation conditions until some station downstream of the tube entrance. Thus, the distance from the heater entrance to the station where saturation conditions prevail is greater than zero (see definition of saturation length, appendix B). It was observed that the tube wall temperature increased and pressure decreased until the saturation-length station was reached. Beyond this point the tube temperature diminished in the manner previously described. It is interesting to observe that, if the hydrogen entered the test section at saturation conditions or with quality, the tube temperatures in the inlet of the heated section would be lower than if the hydrogen were a subcooled liquid. (See runs 18-6 and 18-7, fig. 3(a); also note $\dot{w}$ and p_{in} differences, table I.) One can conclude that lowering the system pressure (lowering the subcooling) would help the cooling process at the inlet if a subcooled fluid were present. (See runs 20-1, 20-2, and 20-3, fig. 3(a), and compare subcooling through use of table I and fig. 8(a).)

The second exception to the monotonically decreasing wall temperature involves an abrupt increase in wall temperature beyond the midportion of the tube. The effect was most noticeable with the 0.625-inch tube. Figure 3(b) shows this wall temperature profile. The figure also shows how this condition grew with increasing heat flux. The abrupt temperature change appeared to take place when the estimated quality reached approximately 50 percent or greater. A similar phenomenon has been observed with water and other fluids in boiling processes (ref. 3), and it is called "vapor binding" or "dry wall." So much vapor is present near the heating surface that in the turbulent vapor-liquid mechanism practically no liquid particles get near enough to the wall to absorb the heat of vaporization. The heat being transferred appears principally as sensible heating of the vapor phase, and the heat-transfer coefficient more closely approaches the single-phase gaseous value.

Pressure Drop

The heated portion of the Inconel test section was instrumented with four pressure taps. The pressure-drop profiles obtained for several flow rates and heat fluxes are shown in figure 4. The pressure drop per unit length may be obtained, with slight modifications, from (ref. 10)

$$\frac{dp}{dL} = -\left[\frac{f}{2}\left(\frac{\rho u^2}{r_i g_c}\right) + \rho\left(\frac{g}{g_c}\right) + \left(\frac{\rho u}{g_c}\right)\left(\frac{du}{dL}\right)\right] \qquad (1)$$

Because of the appreciable difference between the apparent density of the fluid at the entrance and at the exit, the pressure drop could be ascribed to momentum change, and the viscous shear forces at the wall could be neglected. Thus, the form can be simplified to the one-dimensional momentum equation:

$$-\Delta p = \frac{\dot{w}}{Ag_c} \Delta u \qquad (2)$$

The simplified form predicts pressure-drop values that are roughly equivalent to the experimental values. The dashed lines calculated using the one-dimensional relation are superposed on the experimental data of figure 4 to illustrate the relative agreement of analysis and experiment.

Heat Transfer

Local values of heat-transfer coefficient h are plotted as a function of the test-section length for various mass-flow rates and heat inputs in figure 5. These are typical data for both test sections and were selected to show how the coefficient changes with heat flux as well as weight flow. These coefficients for the 0.375-inch tube are also tabulated in table I. The heat-transfer-coefficient results for the smaller-diameter test section were judged to be the more reliable because the local pressures were known throughout the test section.

Several empirical correlation schemes similar to those appearing in references 2 and 3 were applied to the two-phase experimental heat-transfer results. In reference 2 the Martinelli parameter X_{tt} and a modified Reynolds number involving the mass fraction of vapor x were used in establishing the correlation. Similar parameters were chosen for the correlation of the hydrogen data.

First, it has to be established that the Martinelli flow parameter was applicable to the two-phase hydrogen flow model. In the original development of the parameter (ref. 1), the fluid model consisted of a gaseous core and a liquid annulus adjacent to the wall. By a similar derivation it was apparent that the Martinelli parameter was applicable to the hydrogen flow composed of a liquid core and a gaseous annulus (see appendix D).

Several methods of computing a modified Reynolds number for the two-phase flow were tried. The fluid properties were evaluated at various temperatures including wall, bulk, and film (the arithmetic mean of bulk and wall) conditions. These Reynolds numbers, along with corresponding Prandtl numbers, were used in calculating an estimated Nusselt number by the modified Dittus-Boelter equation:

$$Nu_{calc,f} = 0.023\ Re^{0.8} Pr_f^{0.4} \tag{3}$$

In selecting a Reynolds number that would apply to a broad range of qualities (mass-percent vapor), the Reynolds number should be equivalent to a gaseous one when the fluid approaches the single-phase gaseous condition. It was found that this requirement could be satisfied by defining Reynolds number in the following way:

$$Re = \frac{\rho_{f,m} u_{av} D}{\mu_f} \tag{4}$$

where the mean density of the film is

$$\rho_{f,m} = \frac{1}{\frac{x}{\rho_f} + \frac{1 - x}{\rho_l}} \tag{5}$$

x is quality (greater than zero, as discussed later), ρ_f is the gaseous density evaluated at film conditions, ρ_l is the saturated liquid density, u_{av} is the average velocity of the mixture of liquid and gaseous phases, and μ_f is the viscosity at gaseous film conditions.

In addition, writing the density as $\rho_{f,m}$ modifies the film density for the liquid droplets present. Perhaps these droplets, diffusing toward the hot wall, are partially vaporized and then "bounced" back into the core. At high qualities, apparently very small amounts of diffusing liquid are present in the film; thus, the mean film density approaches the gaseous value.

Figure 6 shows a ratio of the experimental Nusselt number to the predicted Nusselt number (based on the preceding definition of Reynolds number) plotted as a function of X_{tt}. The data points represent local conditions at four axial stations near the midportion of the small-diameter Inconel test section. Such a selection of axial stations obviated the end effects. The data may be represented by the following equation:

$$Nu_{exp,f} = \frac{Nu_{calc,f}}{0.611 + 1.93\ X_{tt,f}} \tag{6}$$

Equation (6) is a least-squares fit to the data from $L = 5.86$ to 9.4 inches and is valid for qualities from 0.05 to 0.9 over the range of pressures covered by this report. The equations may be extended, with reservation, to qualities of 0.01 (see fig. 7).

It should be noted that the true case is probably neither a separate phase flow as assumed in the derivation of X_{tt} nor a homogeneous flow as implied by the introduction of x in $\rho_{f,m}$. Hence,

the incorporation of both parameters based upon these extreme cases gave correlation (6).

As quality increases (X_{tt} decreases), the ratio of Nusselt numbers begins to approximate unity. However, a careful look at figure 6 shows the Nusselt number ratio to be greater than unity at the low X_{tt} values. Apparently the presence of nonequilibrium quantities of colloidal particles alters the single-phase gaseous heat-transfer mechanism. It is expected that the experimental values of Nusselt number would equal the predicted values when the flow is strictly single-phase gaseous, as shown by reference 11. Similar results were obtained for helium in reference 12.

It is fairly obvious that the gaseous film density cannot be assigned to the Reynolds number when the fluid is approaching the completely liquid state. Somewhere at high values of X_{tt}, low quality, the Reynolds number should be redefined incorporating liquid properties. Figure 7 includes the families of local data over the tube length. The axial stations included in the correlation begin about 0.625 inch from the inlet (or where saturation occurs) and end 1.6 inches before the tube exit. A least-squares fit to these data yields

$$Nu_{exp,f} = \frac{Nu_{calc,f}}{0.706 + 1.60\ X_{tt,f} - 0.123\ X_{tt,f}^2}$$

This equation and equation (6) are superimposed on the data of figure 7 for comparison.

The families may be represented by equation (6) with the following observations:

(1) The predicted value of Nusselt number is usually lower than the experimental at the inlet and higher at the exit. This tendency in the Nusselt number suggests that a length-diameter-ratio correction might improve the correlation. Additional tube geometries would be required to establish the effect of the L/D term experimentally. Consequently, no attempt to suggest an L/D correction is presented herein.

(2) The correlation applies for moderate subcooling at the pressures considerably below critical and to lower degrees of subcooling as the pressure is increased. The sensitivity of the correlation to the subcooling is much more pronounced near the critical pressure.

As was mentioned in the INTRODUCTION, X_{tt} is a measure of the fluid resistance of the two-phase flow. It has been used to correlate two-phase fluid-flow pressure drop. In its use as a parameter for two-phase heat-transfer correlations, it may be interpreted as a correction to the shear terms in the Dittus-Boelter equation.

A design procedure is treated in some detail in appendix E. This procedure, while nearly comprehensive, must necessarily be modified by the designer to suit the particular application.

SUMMARY OF RESULTS

1. The turbulent two-phase para-hydrogen heat-transfer data are correlated using the Martinelli parameter $X_{tt,f}$ and the modified Dittus-Boelter equation $Nu_{calc,f}$. The data are represented by

$$Nu_{exp,f} = \frac{Nu_{calc,f}}{0.611 + 1.93\ X_{tt,f}} \tag{6}$$

where

$$Nu_{calc,f} = 0.023\ Re^{0.8} Pr_f^{0.4} \tag{3}$$

and

$$Re = \frac{\rho_{f,m} u_{av} D}{\mu_f} \tag{4}$$

Equation (6) holds at least over the range of conditions studied: inlet pressure, 30 to 70 pounds per square inch absolute; average heat flux, 1 Btu per square inch per second maximum; and temperature differential, 50° to 750° R between fluid and wall.

2. Wall temperature profiles were generally high at the inlet and decreased toward the exit; this trend is just the opposite of that usually observed for convective heat transfer with single-phase fluids.

3. Pressure-drop measurements indicated momentum losses to be greater than frictional loss. A one-dimensional momentum analysis can be used to predict pressure drop.

4. Heat absorption due to para-ortho conversion is small and at least within the accuracy of the experiment.

5. Appendixes present justification of assumptions, methods of calculation, para-ortho hydrogen conversion analysis, and a design procedure.

Lewis Research Center
National Aeronautics and Space Administration
Cleveland, Ohio, January 11, 1961

APPENDIX A

SYMBOLS

A	area, sq ft
b	material thickness
C	concentration, (g-mass)(mole)/cc
C_p	specific heat, Btu/(lb-mass)(^oR)
$\bar{C}_p$	mean specific heat, Btu/(lb-mass)(^oR)
D	tube diameter, in.
$\mathscr{D}$	diffusion coefficient
f	Fanning friction factor
g	acceleration due to gravity, ft/sec^2
g_c	conversion constant, 32.174 (lb-mass/lb-force)(ft/sec^2)
ΔH	heat of conversion, (g-mass)(cal)/(g-mass)(mole)
h	heat-transfer coefficient, Btu/(sq in.)(sec)
K	constant
K_{eq}	equilibrium constant
k	reaction rate, sec^{-1}
k_1, k_2	reaction-rate constants, cm/sec
L	local test-section station, in.
L_t	test-section length, in.
l	distance from inlet of heated section to point where saturation conditions occur, in.
m	mass fraction of vapor existing at inlet
m,n	exponents

$Nu_{calc,f}$	Nusselt number computed from modified Dittus-Boelter equation using film temperature to evaluate properties (eq. (3))
$Nu_{exp,f}$	experimental Nusselt number, $h_{exp}D/\kappa_f$
n_v	number of voltage taps
Pr	Prandtl number, $C_p\mu/\kappa$
p	static pressure, lb/sq in. or mm Hg
$\Delta p/\Delta L$	pressure gradient, (lb/sq in.)/in.
Q	heat flow, Btu/sec
q	heat flux, Btu/(sq in.)(sec)
R	gas constant, 82.05 (atm)(cc)/(g-mass)(mole)(^oK)
Re	Reynolds number (eq. (4))
$\mathscr{R}$	conversion rate, (g-mass)(mole)/(cm^2)(sec)
r	tube radius, in.
T	temperature, ^oR or ^oK
ΔT	temperature difference, ^oR or ^oK
t	time, sec
u	velocity, ft/sec
V	volume, cc
$\dot{w}$	mass-flow rate, lb-mass/sec
x	quality, percent vapor by mass
y	distance from wall
α	form factor, liquid area
β	form factor, gaseous area
γ	correction coefficient for hydraulic diameter
δ	boundary-layer thickness, cm
ϵ	emissivity

ζ	isothermal friction factor
κ	thermal conductivity, Btu/(ft)(sec)(^{o}R)
κ_M	thermal conductivity of material, Btu/(ft)(sec)(^{o}R)
λ	heat of vaporization, Btu/lb-mass
μ	viscosity, lb-mass/(ft)(sec)
ρ	density, lb-mass/cu ft
$\rho_{f,m}$	mean film density (eq. (5)), lb-mass/cu ft
σ	Stefan-Boltzmann constant, 0.173×10^{-8} Btu/(hr)(sq ft)(^{o}R^4)
τ	half-life, sec
X_{tt}	Martinelli two-phase parameter (both phases turbulent) (eq. (D16))

Subscripts:

av	average
b	bulk temperature
Cu	copper
can	vacuum container enclosing test section
e	exit
eq	equilibrium
exp	experimental
F	flange
f	film conditions, arithmetic mean between wall and bulk temperature
g	gas
i	inside wall of test section
in	inlet

L	station along heated length
l	liquid
o	outside wall of test section
or	orifice
ortho	ortho-hydrogen
para	para-hydrogen
pipe	test section
R	radiation
sat	saturation
t	time
tot	total
tp	two phase
V	Venturi
v	voltage tap
W	voltage-tap wire
w	wall
3	thermocouple location 1/2 inch from flange
4	thermocouple location at flange
5	instrumentation junction strip

APPENDIX B

COMPUTATIONAL PROCEDURE

Inside-Wall Temperature

The tube surface thermocouples were mounted on the exterior surface. Values of the inside-wall temperature were computed from the following expression (ref. 13), which presupposes uniform radial heat flux through the tube wall (tube generating power):

$$T_i = T_o - Z \frac{Q}{K_M}$$

where

$$Z = \frac{r_o^2 \ln \frac{r_o}{r_i} - \left(\frac{r_o^2 - r_i^2}{2} \right)}{2\pi L \left(r_o^2 - r_i^2 \right)}$$

Saturation Length

Before computing the local density and quality of hydrogen at any axial station in the tube, some simplifying assumptions are required to establish where vapor accumulation begins.

It is recognized that, for the rather appreciable differences between the wall and the bulk temperatures, boiling probably begins at the entrance of the test section. However, if the local bulk temperature in the tube entrance is less than the saturated temperature, subcooled boiling occurs. For most of the actual experimental runs, some degree of subcooling at the entrance was prevalent.

In computing the quality of the hydrogen at any axial station in the tube, it was assumed that an unappreciable amount of vapor was generated when the bulk was subcooled. This assumption is valid for low subcooling. Thus, quality was assumed to appear in the tube only when saturation conditions were reached. A saturation length l has been defined as the axial distance from the entrance of the tube to the location of saturation conditions. In computing l, the bulk temperature and pressure profiles are required. The pressure profiles were obtained from the data, and the bulk temperature profiles were obtained by computation:

$$T'_{b,L+1} = T_{b,L} + \frac{Q}{L_t \dot{w}} \frac{\Delta L}{\bar{C}'_p}$$

where $\bar{C}'_p$ is evaluated at $T_{b,L}$;

$$\Delta L = L_{L+1} - L_L$$

$$T_{b,L+1} = T_{b,L} + \left(\frac{Q}{L_t \dot{w}}\right) \frac{\Delta L}{\bar{C}_p} \qquad \text{(B1)}$$

where $\bar{C}_p$ is evaluated at $(T'_{b,L+1} + T_{b,L})/2$.

To each pressure there corresponds a saturation temperature; thus, l may be computed by locating the first station where $T_{b,L} \geq T_{b,L,sat}$ ($T_{b,L,sat}$ based on p_L), retiring one station, computing Δl, and adding the station length (see sketch).

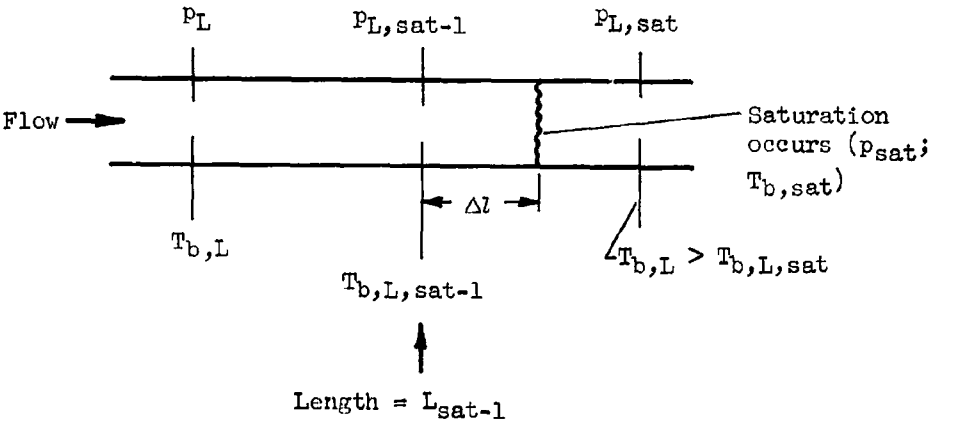

The pressure drop, to obtain Δl, was computed from

$$p_{L,sat} = p_{L,sat-1} - \frac{\Delta p}{\Delta L} \Delta l$$

where

$$-\frac{\Delta p}{\Delta L} = \frac{p_{L,sat-1} - p_{L,sat}}{L_{sat} - L_{sat-1}} \qquad \text{(B2)}$$

Using (B1), (B2), and an exponential or polynomial function to describe p_{sat} as a function of $T_{b,sat}$, an iterative process yields $T_{b,sat}$. Then,

$$\Delta l = \frac{T_{b,sat} - T_{b,L,sat-1}}{\left(\frac{Q}{L_t \dot{w} C_p}\right)}$$

and

$$l = L_{sat-1} + \Delta l \qquad \text{(B3)}$$

Reference 14 presents an experimental study of the void fraction (flow area occupied by vapor) for water at 2000 pounds per square inch, which is pertinent to the definition of l. The attenuation of gamma rays was the experimental technique used to measure the void distribution. Appreciable quantities of vapor were measured for subcooled boiling. Heat flux and the model of the two-phase flow (whether stratified or diffuse) had a marked influence on correlating the void fraction with the quality.

While these water data cannot be applied directly to boiling hydrogen, they do point out the limitations of the assumption used in computing hydrogen quality. An estimated comparison of the actual quality distribution through the tube with the computed distribution might look like the following sketch:

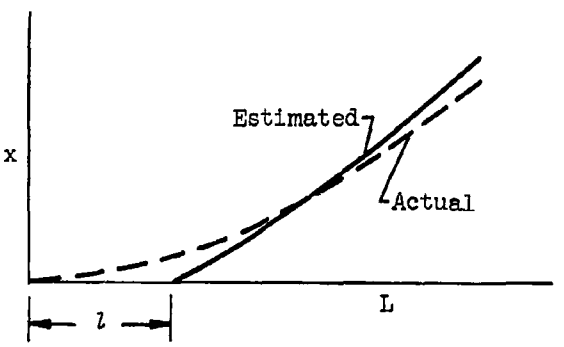

For the data reported herein, the subcooling was moderate and the vapor generated to l was small. The solid curve is not a straight line because the pressure drop through the tube produced a superheat condition, which is favorable for vapor production.

There were a number of experimental runs in which saturation conditions occurred before the fluid reached the heated portion of the test

section. For these cases, a negative l with respect to the test-section inlet was considered. These cases were computed separately from those in which l was positive and will be treated in the discussion of quality.

It is speculated that the analysis used is relatively accurate in the midportions of the tube, the portion used for the heat-transfer results. The quality in the subcooled entrance region and in the exit section, where a vapor layer and end losses reduce the production of additional vapor, will not be predicted accurately.

Quality

The quality downstream of the saturation length is computed from

$$x = \frac{Q}{L_t \dot{w}} \left(\frac{L_t - l}{\lambda} \right) \tag{B4a}$$

For the experimental runs in which saturated conditions existed upstream of the heated test section, l, in (B4a), was taken as zero, and a mass fraction of vapor m was added to give the local quality:

$$x = \frac{Q}{L_t \dot{w}} \left(\frac{L_t}{\lambda} \right) + m \tag{B4b}$$

The method for computing m can be best explained by referring to the following sketch:

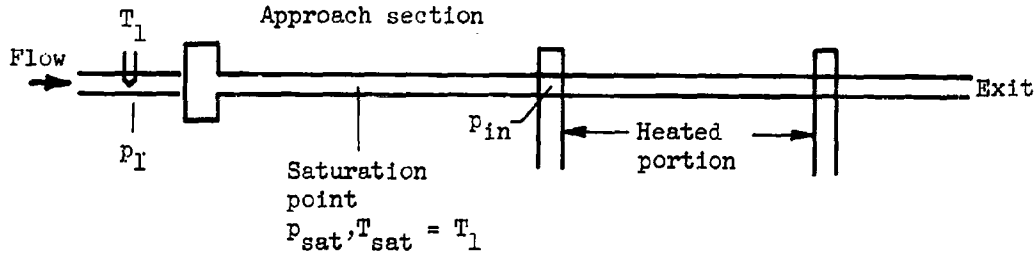

where T_1 is the bulk temperature measurement at the entrance to the test section, and p_1 is the corresponding measured pressure. From the pressure-drop data, a station in the unheated tube is determined where saturation conditions exist. The bulk temperature of the fluid is assumed constant throughout the unheated section up to this point.

The enthalpy change from the saturation point to the heated tube inlet caused by evaporation is approximately the difference in the saturated liquid enthalpies between these stations. Since the properties change little in the approach section, one may determine the quality at the entrance by

$$m = \frac{\bar{C}_p(T_{sat} - T_{in})}{\lambda} \tag{B5}$$

where $\bar{C}_p$ is the specific heat evaluated at $(T_{sat} + T_{in})/2$, $T_l = T_{sat}$ = bulk temperature, and T_{in} = saturated bulk temperature at inlet (based on pressure). There were no runs where saturation occurred before the approach section.

Density and Velocity

The density at any axial station can be computed from knowledge of the quality:

$$\rho_b = \frac{1}{\frac{x}{\rho_{g,sat}} + \frac{1 - x}{\rho_{l,sat}}} \tag{B6}$$

The local velocity may now be computed from one-dimensional continuity:

$$u_{av} = \frac{\dot{w}}{\rho_b A} \tag{B7}$$

Estimation of Heat Losses

Since no experimental method was used in measuring the heat losses, they had to be estimated. To facilitate the calculation, only very simplified geometries were used. It was found that, among all the possible causes for heat loss, the major ones were radiation loss, heat loss through the electrical copper flanges, and heat loss through copper voltage taps.

Radiation loss. - The radiation from the body at T_o to an enveloping body at T_{can} is the radiation heat loss:

$$Q_R = \frac{\sigma A_o \left(T_o^4 - T_{can}^4\right)}{\frac{1}{\epsilon_o} + \left(\frac{r_o}{r_{can}}\right)\left(\frac{1}{\epsilon_{can}}\right) - 1} \tag{B8}$$

where the temperature of the stainless-steel vacuum container T_{can} is taken as 500° R, the radius r_{can} is 7.5 inches, and the emissivity ϵ_{can} is 0.5.

Conduction loss through flanges. - A first approximation to the axial conduction through one end of a hollow cylinder with power generated in the cylinder is as follows:

$$Q_F = 2\,\frac{\pi\left(r_o^2 - r_i^2\right)K_M(T_3 - T_4)}{\frac{L_3 - L_4}{2}} \tag{B9}$$

where r_o is 0.1875 and 0.313 inch and r_i is 0.1565 and 0.248 inch for the 0.375- and the 0.625-inch tubes, respectively; the thermal conductivity of Inconel or stainless steel K_M is approximately 2×10^{-4} Btu/(in.)(sec)(°R); and $L_3 - L_4$ is 0.5 inch.

Conduction loss through voltage taps. - Conduction through a slim rod is obtained as follows:

$$Q_v = n_v \pi r_W^2 K_{Cu} \left(\frac{T_o - T_5}{L_1 - L_5}\right) \tag{B10}$$

where the number of voltage taps n_v is 8, the radius of the voltage-tap wire r_W is 1/64 inch, the thermal conductivity of copper K_{Cu} is 4.63×10^{-4} Btu/(in.)(sec)(°R), the temperature of the junction strip for instrumentation within the vacuum jacket $T_5 = (T_o/2) + 250°$ R, and the distance between tube and instrument junction strip $L_1 - L_5$ is 2 inches.

In general, the averaged outside-wall temperature increased with total heat input Q_{tot}, and the term $T_3 - T_4$ shows the same trend. The following table summarizes the estimates of various forms of heat loss from the Inconel tube as a function of total heat input Q_{tot}:

	Q_{tot}, Btu/sec				
	2.7	4.6	7.1	9.9	12.0
T_o, °R	270	390	520	630	680
$T_3 - T_4$, °R	100	170	210	290	330
Heat loss[a], Btu/sec:					
Q_R	-0.0021	-0.0014	0.0007	0.0038	0.0059
Q_F	.006	.0088	.0118	.0155	.0185
Q_V	-.00018	-.0008	0	.0008	.0013
ΣQ_{loss}, Btu/sec	0.0037	0.0066	0.0125	0.0201	0.0257
Percent loss	0.137	0.143	0.176	0.203	0.214

[a]Negative sign denotes flow of heat into test section.

The tabulated values of heat losses indicate that data corrections for heat loss are not warranted.

APPENDIX C

PARA-ORTHO CONVERSION

Because of the strange shapes of wall temperature profiles encountered in the boiling of liquid hydrogen, questions were raised as to the possible effect on the heat transfer of the conversion of para-hydrogen (p-H_2) to ortho-hydrogen (o-H_2). This speculation was based upon the following considerations:

(1) The liquid hydrogen used contained about 95 percent p-H_2, while the equilibrium concentrations of p-H_2 are 50 percent at 138° R and 25 percent at 540° R.

(2) The heat of reaction for para-ortho conversion is known to be comparable to the latent heat of vaporization at or near the boiling point. In addition, the specific heat and thermal conductivities of the two modifications of hydrogen are quite different when the temperature is below 650° R.

Mechanism of Para-Ortho Conversion

In order to estimate the effect of this para-ortho conversion, it is necessary first to examine the associated mechanisms and then to determine which one may apply to the experimental system.

The para-ortho conversion may take place in the following forms:

(1) Homogeneous reactions:

(a) Direct transition: A very slow reaction, about one transition every 300 years.

(b) Collision of molecules: Half-life time is 3 years.

(c) Collision with hydrogen atoms (H): The H atoms may be generated by photons, electric charges, alpha rays, and gamma rays. But it is also a very unfavorable reaction for ortho to para conversion at 138° R (see ref. 15). Since no radiation source exists in the hydrogen heat-transfer apparatus, this reaction mechanism is eliminated.

(2) Heterogeneous reactions:

(a) Paramagnetic mechanism: The H_2 molecule is absorbed and the spin is reversed (ref. 16). Catalysts for this process are paramagnetic oxides, charcoal with traces of impurities, and others.

(b) Chemisorption: H_2 molecules are chemisorbed on metal films and activated (ref. 16). The bonds between H atoms are broken and recombined. Thus, a good catalyst must have a strong chemisorption property toward H_2. Among the active chemisorption materials mentioned in reference 17 are tungsten, nickel, tantalum, and tellurium. Thus, it follows that stainless steel and Inconel should be good catalysts. Since the tube wall is the hottest spot in the apparatus, the para-ortho conversion should take place at the stainless-steel tube wall if there is any such reaction.

Based upon the preceding survey, it appears that investigation about the possibility of para-ortho conversion should be directed toward the reaction at the wall.

Conversion Rate in Heterogeneous Reactions

The mechanism for conversion can be assumed to occur as follows:

(1) Diffusion of p-H_2 through a boundary layer to the wall

(2) p-H_2 to o-H_2 on the catalytic wall

(3) Diffusion of o-H_2 out through the film

By assuming the para-ortho conversion to be a first-order reaction,

$$-k_1 C_{ortho,w} + k_2 C_{para,w} = \mathscr{D}_w \frac{dC_{para}}{dy} \tag{C1}$$

where k_1 and k_2 are absolute reaction-rate constants, $\mathscr{D}$ is the diffusion coefficient, and y is the distance from the wall. With the assumptions of a linear concentration profile across the boundary layer of thickness δ and $C_{para,b} \gg C_{ortho,b}$, it can be shown that

$$\mathscr{R} = \frac{\frac{\mathscr{D}}{\delta} K k_1 C_{para,b}}{(1 + K_{eq})k_1 + \frac{\mathscr{D}_w}{\delta}} \tag{C2}$$

where $\mathscr{R}$ is reaction rate of moles per unit area per unit time; b refers to bulk temperature; K_{eq} is the equilibrium constant at wall temperature, $C_{ortho,w}/C_{para,w}$; and $K_{eq} = 3$ for $T > 350^\circ$ R.

If the analogy between heat transfer, mass transfer, and momentum transfer is used (ref. 9), it can further be shown that

$$h_{overall} = h_{thermal}\left[1 + \frac{(K_{eq}\sqrt{f_c Pr})\,\frac{k_1}{C_p\rho}\,C_{para,b}\left(\frac{\Delta H}{\Delta T}\right)}{(1 + K_{eq})k_1 + h_{thermal}\,\frac{\sqrt{f_c Pr}}{C_p\rho}}\right] \qquad (C3)$$

or

$$h_{overall} = h_{thermal} + \frac{\Delta H \mathscr{R}}{\Delta T}$$

where $h_{overall}$ is the overall heat-transfer coefficient, $h_{thermal}$ is that for the case without para-ortho conversion, and $f_c = \mathscr{D}\rho/\mu$ is a constant (f_c = 1.28 to 1.37).

However, since in most practical cases the wall temperature is near or above 540° R where ΔH is very small, the contribution to the heat transfer due to para-ortho conversion must be negligible. Thus, even if there is some conversion, the only effects on heat transfer will be related to changes in the magnitude of C_p and transport properties. As to $T_w < 540°$ R, ΔH is not zero, and equation (C3) may still give some information about this additional heat transfer due to conversion.

Estimation of Reaction Rate

To weigh the effects of the secondary factors such as differences in thermal conductivities and specific heats, it is instructive to estimate the reaction rate. Equation (C2) may be used if k_1 is known. However, because of the lack of data, k_1 is not readily available. The only information that is useful is an experimental determination of half-life time τ for para concentration at a nickel wire with surface area of 1/2 square centimeter and the gas volume at 773° K and p = 100 millimeters of mercury. These half-life data will be used to estimate reaction rates. From reference 9,

Temp., T, °K	Half-life, τ, sec
323	5000
398	2000
423	800
448	500
473	150

It was further shown in reference 9 that

$$\tau p^{-0.4} = \text{constant} \tag{C4}$$

This information is, of course, far from adequate. But to get a first-order estimate, this is better than nothing. Further, it should be noticed that, since no information was available as to the thickness of film, and so forth, application of these data also implies the assumption that diffusion rate in this experiment was about the same as the one in the present system.

In reference 9,

$$\frac{dC_t}{dt} = -k(C_t - C_{eq}) \tag{C5}$$

where C_t refers to concentration at time t, and k refers to reaction rate. In terms of moles converted per unit time and area, then,

$$\mathscr{R} = \frac{kV}{A}(C_{t,para} - C_{eq,para}) \text{ at } T_w$$

$$= k'(C_{t,para} - C_{eq,para}) \tag{C6}$$

where

$$k' = \frac{kV}{A} = \frac{\ln 2}{\tau}\left(\frac{V}{A}\right)$$

But, for the experimental system,

$$V = 500 \text{ cc}, \quad A = 0.5 \text{ sq cm}$$

Therefore,

$$k' = \frac{(\ln 2)\,\frac{500}{0.5}}{\tau} = \frac{693}{\tau} \quad \text{cm/sec}$$

Suppose

$$T_w = 852^{\circ} \text{ R}, \quad \tau = 150 \text{ sec}, \quad p = 100 \text{ mm}$$

At conditions where p = 800 millimeters, using equation (C4), τ is

$$\tau = 150\left(\frac{800}{100}\right)^{0.4} = 344 \text{ sec}$$

Further, at

$$T_w = 852^\circ \text{ R}, \quad p = 800 \text{ mm}$$

then

$$C_{t,para} = \frac{p}{RT_w} \text{ (100\% para from bulk)}$$

$$C_{para,eq} = 0.25 \frac{p}{RT_w}$$

Thus,

$$\mathscr{R} = \frac{693}{344}(1 - 0.25)\left(\frac{800}{760}\frac{1}{82.05}\frac{1.8}{852}\right)$$

$$= 4.1\times10^{-5} \text{ g-mole/(cm}^2\text{)(sec)} = 0.6 \text{ lb/(sq ft)(hr)}$$

At a wall temperature of 500° R, ΔH due to para-ortho conversion will be small, ΔT large, and $\mathscr{R}$ small; therefore,

$$h_{thermal} \approx h_{overall}$$

Knowing $\mathscr{R}$, the total weight converted at a specific flow rate can be estimated. The total conversion rate in a 12-inch-long, 1/2-inch-inside-diameter tube becomes

$$\mathscr{R}_{tot} = 0.6\left(\frac{\pi/2}{12}\right)(1) = 0.0785 \text{ lb/hr}$$

For a flow rate of 0.1 pound per second, the weight percent converted is

$$\frac{0.0785}{3600(0.1)} \approx 0.022\%$$

Thus, para-ortho conversion should have no effect on the experimental data.

Experimental Results

Since the para-ortho conversion is endothermic, it should help the heat transfer; and thus the stainless-steel tube should be expected to show a lower wall temperature than a gold-plated tube. But the experimental data showed the gold-plated tube to give a lower wall temperature.

Therefore, the deviation between the two profiles of wall temperature is more likely to be due to experimental error than to para-ortho conversion.

Conclusions

(1) The para-ortho conversion should take place on catalytic tube walls.

(2) The reaction rate was estimated to be negligible in the present system. Further, because of low heat of reaction, the effect on heat transfer, if any, should be only secondary.

(3) Experimental results with different surface materials showed no effect of the presence or absence of a catalytic surface.

APPENDIX D

MARTINELLI PARAMETER X_{tt}

Introduction

One of the variables used in correlating the data is the Martinelli two-phase parameter X_{tt}. The two-phase pipe-flow model was composed of a cylindrical gaseous core and a liquid annulus around it flowing along the wall isothermally. The general form of the two-phase pressure-drop equation is

$$\left(\frac{\Delta p}{\Delta L}\right)_{tp} = \left(\frac{\Delta p}{\Delta L}\right)_{g}(Y, X_{tt}) \qquad (D1)$$

The parameter Y must be determined experimentally and is a correction coefficient for the hydraulic diameter of annular flow and the velocity of one phase relative to the other. Martinelli interprets the X_{tt} parameter as an index of the wall and two-phase shear resistance of the two-phase flow.

There are two differences in the two-phase hydrogen flow model as compared with Martinelli's original model. First, heat transfer is present, whereas Martinelli considered only an isothermal case. The presence of heat transfer would affect the magnitude but not the definition of the friction factor. (Martinelli used the Blasius equation.)

Second, the hydrogen gas phase is adjacent to the wall, and the liquid phase makes up the core. This is an inversion in the position of the phases in the pipe as specified by Martinelli. However, it is shown that the same two-phase parameter X_{tt} evolves from the subsequent analysis, which is quite similar to that of Martinelli.

Martinelli Two-Phase Analysis

The principal assumptions used in reference 1 are:

(A) Gas-phase $\Delta p/\Delta L$ equals liquid-phase $\Delta p/\Delta L$.

(B) Volume of gas plus volume of liquid equals volume of pipe at any instant.

The pressure drops (gas and liquid) can be expressed by the Weisbach equation (ref. 1):

$$\left.\begin{aligned} -\left(\frac{\Delta p}{\Delta L}\right)_{tp,l} &= \zeta_l \frac{\rho_l}{D_l} \frac{u_l^2}{2g_c} \\ -\left(\frac{\Delta p}{\Delta L}\right)_{tp,g} &= \zeta_g \frac{\rho_g}{D_g} \frac{u_g^2}{2g_c} \end{aligned}\right\} \qquad \text{(D2)}$$

Note that the Δp of the two-phase flow is greater than that of either single phase because, in addition to wall friction, there exists a varying gas-liquid interface.

Again recall that Martinelli considered a two-phase system in which the liquid was an annulus flow adjacent to the wall, the gas phase constituting the core. Defining the hydraulic diameter for cylindrical flow as

$$\frac{\pi}{4} D^2 = A$$

where A is the area encompassed by the fluid, Martinelli wrote expressions for the effective hydraulic diameter of each phase:

$$\left.\begin{aligned} A_l &= \frac{\alpha \pi D_l^2}{4} \\ A_g &= \frac{\beta \pi D_g^2}{4} \end{aligned}\right\} \qquad \text{(D3)}$$

where α and β are form factors and in effect ratios of the actual cross-sectional area to a circular cross section. For his flow model, Martinelli argued that $\beta \approx 1$ and $\alpha \gg 1$. For the hydrogen flow, $\alpha \approx 1$ and $\beta \gg 1$; thus, some modification to his presentation is necessary.

Assuming $\alpha = 1$ and $\beta \neq 1$, the mean fluid velocities may be computed from

$$\left.\begin{aligned} u_l &= \frac{4\dot{w}_l}{\pi D_l^2 \rho_l} \\ u_g &= \frac{4\dot{w}_g}{\beta \pi D_g^2 \rho_g} \end{aligned}\right\} \qquad \text{(D4)}$$

where $\dot{w}_l$ and $\dot{w}_g$ are flow rates of the liquid and gas, respectively. Martinelli notes that, strictly speaking, equations (D4) cannot be substituted in equations (D2). However, the experimental determination of β or α corrects for this situation. The velocities in equations (D2) should involve the velocity of one phase relative to the other.

The isothermal friction factors ζ_l and ζ_g may be expressed in the generalized Blasius form:

$$\left.\begin{aligned} \zeta_l &= \frac{\left(\frac{\pi}{4}\right)^n K_l}{\left(\frac{\dot{w}_l}{D_l \mu_l}\right)^n} \\ \zeta_g &= \frac{\left(\frac{\pi}{4}\right)^m K_g}{\left(\frac{\dot{w}_g}{\beta D_g \mu_g}\right)^m} \end{aligned}\right\} \qquad \text{(D5)}$$

where K_l and K_g are empirical constants. For the case where both phases are turbulent,

$$K_g = K_l = 0.184$$

$$n = m = 0.2$$

Similar friction factors for nonisothermal conditions may be defined, and the constants change. Using equations (D2) and substituting equations (D3) to (D5),

$$-\left(\frac{\Delta p}{\Delta L}\right)_{tp,l} = \frac{\left(\frac{\pi}{4}\right)^n K_l}{\left(\frac{\dot{w}_l}{D_l \mu_l}\right)^n} \left(\frac{\rho_l}{D_l}\right)\left(\frac{1}{2g_c}\right) \frac{\dot{w}_l^2}{\left(\frac{\pi}{4} D_l^2\right)^2 \rho_l^2} \qquad \text{(D6a)}$$

$$-\left(\frac{\Delta p}{\Delta L}\right)_{tp,g} = \frac{\left(\frac{\pi}{4}\right)^m K_g}{\left(\frac{\dot{w}_g}{\beta D_g \mu_g}\right)^m} \left(\frac{\rho_g}{D_g}\right)\left(\frac{1}{2g_c}\right) \frac{\dot{w}_g^2}{\left(\frac{\pi}{4} D_g^2\right)^2 \rho_g^2} \frac{1}{\beta^2} \qquad \text{(D6b)}$$

Using assumption (A) and equating (D6a) and (D6b), solve for the ratio D_l/D_g and substitute the values for m and n:

$$\left(\frac{D_l}{D_g}\right)^2 = \beta^{0.75}\left(\frac{\dot{w}_l}{\dot{w}_g}\right)^{0.75}\left(\frac{\mu_l}{\mu_g}\right)^{0.083}\left(\frac{\rho_g}{\rho_l}\right)^{0.416} \tag{D7}$$

Using assumption (B),

$$\frac{\pi}{4} D_l^2 L + \frac{\pi}{4} \beta D_g^2 L = \frac{\pi}{4} D_{pipe}^2 L \tag{D8}$$

or

$$D_l^2 + \beta D_g^2 = D_{pipe}^2 \tag{D9}$$

Diameters D_l and D_g are unknowns. Martinelli solved for D_g, which was the diameter of the cylindrical gaseous core. For the hydrogen model, D_l is the diameter of the cylindrical liquid core. Consequently, an expression for this parameter will be found using equation (D7):

$$D_l^2 + \frac{\beta D_l^2}{\beta^{0.75}\left(\frac{\dot{w}_l}{\dot{w}_g}\right)^{0.75}\left(\frac{\mu_l}{\mu_g}\right)^{0.083}\left(\frac{\rho_g}{\rho_l}\right)^{0.416}} = D_{pipe}^2 \tag{D10}$$

or

$$D_l = \frac{D_{pipe}}{\sqrt{1 + \beta^{0.25}\left(\frac{\dot{w}_l}{\dot{w}_g}\right)^{-0.75}\left(\frac{\mu_l}{\mu_g}\right)^{-0.083}\left(\frac{\rho_g}{\rho_l}\right)^{-0.416}}} \tag{D11}$$

This is similar to Martinelli's answer for D_g.

Referring to equation (D6a), it can be shown that

$$-\left(\frac{\Delta p}{\Delta L}\right)_{tp} = \left[K_l\left(\frac{\pi}{4}\right)^{n-2}\left(\dot{w}_l^{2-n}\right)\left(\frac{1}{D_{pipe}^{5-n}}\right)\left(\frac{\mu_l^n}{\rho_l}\right)\left(\frac{1}{2g_c}\right)\right]\frac{D_{pipe}^{5-n}}{D_l^{5-n}} \tag{D12}$$

Thus,

$$\left(\frac{\Delta p}{\Delta L}\right)_{tp} = \left(\frac{\Delta p}{\Delta L}\right)_l \left(\frac{D_{pipe}}{D_l}\right)^{5-n}$$

$$= \left(\frac{\Delta p}{\Delta L}\right)_l \left(\frac{D_{pipe}}{D_l}\right)^{4.8} \qquad \text{(D13)}$$

Using equation (D11),

$$\left(\frac{\Delta p}{\Delta L}\right)_{tp} = \left(\frac{\Delta p}{\Delta L}\right)_l \left[1 + \beta^{0.25}\left(\frac{\dot{w}_l}{\dot{w}_g}\right)^{-0.75}\left(\frac{\mu_l}{\mu_g}\right)^{-0.083}\left(\frac{\rho_g}{\rho_l}\right)^{-0.416}\right]^{2.4} \qquad \text{(D14)}$$

Martinelli obtained a comparable result:

$$\left(\frac{\Delta p}{\Delta L}\right)_{tp} = \left(\frac{\Delta p}{\Delta L}\right)_g \left[1 + \alpha^{0.25}\left(\frac{\dot{w}_l}{\dot{w}_g}\right)^{+0.75}\left(\frac{\mu_l}{\mu_g}\right)^{+0.083}\left(\frac{\rho_g}{\rho_l}\right)^{+0.416}\right]^{2.4} \qquad \text{(D15)}$$

To correlate his results, Martinelli sought a parameter that would produce α for various fluids. It so happened that the multiplier of α in the previous equation did the job. For simplicity, this was called X_{tt}. It represents the shearing force in the two phases.

The X_{tt} parameter was found more convenient to compute if the exponents were changed to more even digits. Raising each term to the 1.2 power does not change the "weight" of each term; thus, X_{tt} was written as follows:

$$\frac{1}{X_{tt}} = \left(\frac{\dot{w}_g}{\dot{w}_l}\right)^{0.9}\left(\frac{\mu_g}{\mu_l}\right)^{0.1}\left(\frac{\rho_l}{\rho_g}\right)^{0.5}$$

$$= \left(\frac{x}{1-x}\right)^{0.9}\left(\frac{\mu_g}{\mu_l}\right)^{0.1}\left(\frac{\rho_l}{\rho_g}\right)^{0.5} \qquad \text{(D16)}$$

In this report, X_{tt} is used rather than the inverse form as would be obtained from equation (D14).

APPENDIX E

DESIGN PROCEDURE

There are many design methods and procedures and many two-phase systems in which the data of this report may be applied; however, only one system will be considered herein.

In applying this correlation to a design problem, such as the channel of a regeneratively cooled rocket engine, the designer should have approximate values for the channel geometry, inlet pressure and temperature, the mass-flow rate, and the combustion-chamber and nozzle properties. With this idea of channel geometry, the designer can then calculate the heat-flux distribution with or without radiation by a method such as that outlined in reference 18. Methods outlined in appendix B will be employed, without further reference, to obtain some of the following design information.

For a first approximation, assume a constant pressure profile, p_{in}.

(a) Determine l by computing the bulk temperature:

$$T_{b,L+1} = T_{b,L} + \left(\frac{Q_2 - Q_1}{L_2 - L_1}\right)\frac{\Delta L}{\dot{w}\bar{C}_p} \tag{E1}$$

where $(Q_2 - Q_1)/(L_2 - L_1)$ is the heat input per unit length, and ΔL is the length between L_{L+1} and L_L. Since $T_{b,sat}$ is known from the pressure (i.e., $p_L = p_{in}$),

$$l = L_{sat-1} + \Delta l \tag{B3}$$

follows immediately. The l estimated in this manner will usually be greater than the actual l, but is a good approximation for low subcooling.

(b) Compute x using λ evaluated at $p = \text{const.} = p_{in}$.

(c) The average density at each station is then estimated using the saturated liquid and gaseous densities. The average density prior to saturation ($l \geq L$) is obtained from the bulk temperatures, previously computed while determining l.

(d) The static pressure at each station is computed using one-dimensional continuity and momentum pressure drop (see also fig. 4):

$$\dot{w} = \rho u A \qquad (E2)$$

$$-\Delta p = \frac{\dot{w}}{A g_c}\,\Delta u \qquad (2)$$

The designer must now iterate the processes of finding x_L, l, ρ_L, p_L, while using p_L to determine $T_{b,L,sat}$ (see fig. 8(a)), until the desired accuracy is attained. After obtaining this information, compute $X_{tt,f}$. Equation (6) will then yield the ratio $Nu_{calc,f}/Nu_{exp,f}$.

Compute $Nu_{calc,f}$ using

$$Nu_{calc,f} = 0.023\, Re^{0.8} Pr_f^{0.4} \qquad (3)$$

and local properties evaluated at film temperature (arithmetic mean between bulk and wall). Transport properties are available in literature from the National Bureau of Standards (refs. 5 to 7). The local heat-transfer coefficient $h_{tp,L}$ now becomes available through $Nu_{exp,f}$ (eq. (6)). Compute the coolant wall temperature accounting for the material and find the heat-flux distribution into the fluid. Since input heat and absorbed heat will generally not agree, an iteration of the entire bulk cooling process will be required to balance the gas-side and liquid-side heat fluxes. One must keep in mind that the $h_{tp,L}$ computed will probably be conservative, since a rocket channel heats only a portion of the wetted perimeter, while in this experiment the entire wetted perimeter was heated.

To recapitulate, using figures and formulas (see text and appendix B for source of equations):

(1) The designer must know something of the geometry and conditions to be met. Consider a single-pass channel:

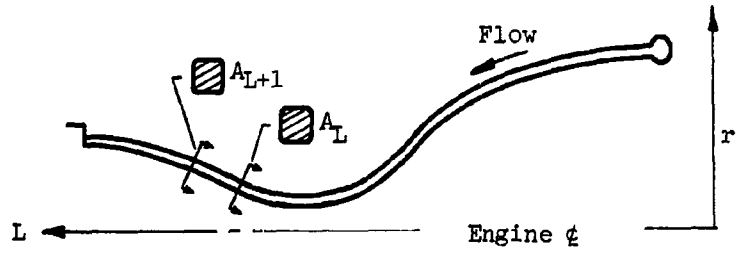

A_L is not necessarily $\geq A_{L+1}$

(2) The heat-flux distribution must be estimated (see ref. 18):

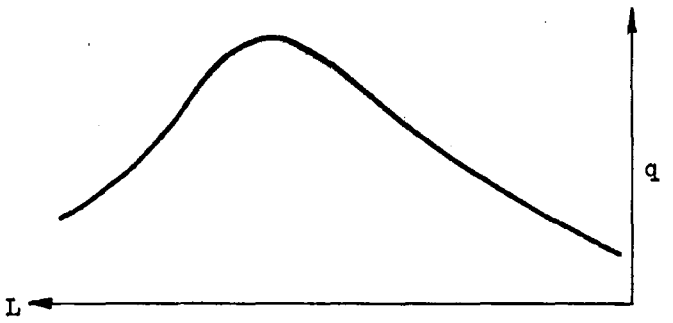

(3) The saturation length may be estimated from

$$T_{b,L+l} = T_{b,L} + \left(\frac{Q_2 - Q_1}{L_2 - L_1}\right)\frac{\Delta L}{\dot{w}\bar{C}_p} \tag{E1}$$

$$l \approx L_{sat-l} + \Delta l \tag{B3}$$

For constant heat input per unit length or saturation prior to heating, see appendix B.

(4) The local quality may now be computed:

$$x = \sum_{l}^{L}\left(\frac{Q_2 - Q_1}{L_2 - L_1}\right)\left(\frac{\Delta L}{\dot{w}\lambda}\right) \tag{E3}$$

and, for constant heat input per unit length,

$$x = \frac{Q}{L_t\dot{w}}\left(\frac{L_t - l}{\lambda}\right) \tag{B4a}$$

(5) The local two-phase density is given by

$$\rho_b = \frac{1}{\frac{x}{\rho_{g,sat}} + \frac{1 - x}{\rho_{l,sat}}} \tag{B6}$$

(6) The local velocity may now be estimated from the one-dimensional continuity equation:

$$u_{av} = \frac{\dot{w}}{\rho_b A} \tag{B7}$$

(7) The local pressure drop is estimated using equation (2):

$$-\Delta p = \frac{\dot{w}}{A g_c} \Delta u \tag{2}$$

(8) Iterate the preceding steps to obtain better approximations for the flow parameters.

(9) The approximated pressure drops may appear as follows:

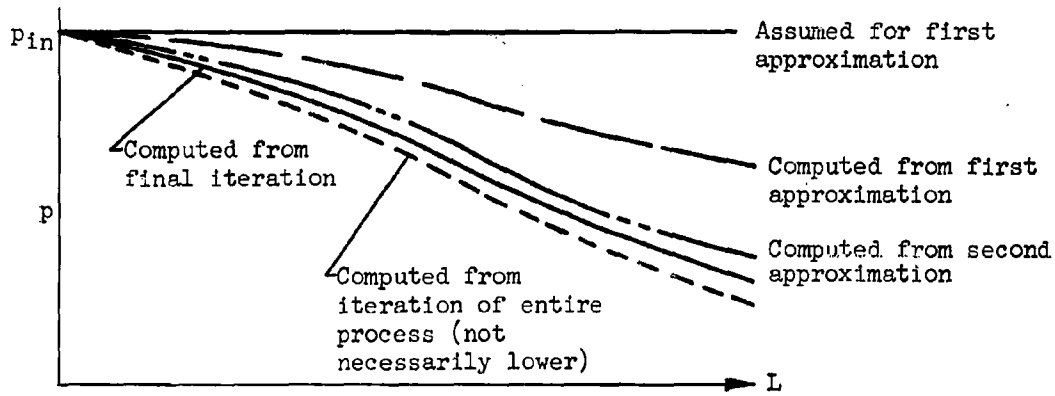

(10) Calculate $X_{tt,f}$ from

$$\frac{1}{X_{tt,f}} = \left(\frac{x}{1-x}\right)^{0.9} \left(\frac{\mu_f}{\mu_l}\right)^{0.1} \left(\frac{\rho_l}{\rho_f}\right)^{0.5} \tag{D16}$$

(11) Estimate the Nusselt number ratio by using equation (6):

$$Nu_{exp,f} = \frac{Nu_{calc,f}}{0.611 + 1.93\, X_{tt,f}} \tag{6}$$

(12) Compute the local Nusselt number using the modified Dittus-Boelter equation:

$$Nu_{calc,f} = 0.023\ Re^{0.8} Pr_f^{0.4} \tag{3}$$

where

$$Re = \frac{\rho_{f,m} u_{av} D}{\mu_f} \tag{4}$$

and

$$\rho_{f,m} = \frac{1}{x/\rho_f + (1 - x)/\rho_l} \tag{5}$$

(13) Using steps (12) and (11), compute the local two-phase heat-transfer coefficient:

$$h_{tp,L} = \frac{1}{D}\left(\frac{Nu_{exp,f}}{\kappa_f}\right)_L \tag{E4}$$

(14) Compute the liquid-side wall temperature $T_{w,L}$ accounting for the wall thickness:

$$T_{w,L} = T_{w,g} - K\frac{q}{\kappa_M b} \tag{E5}$$

Other forms of computing heat transfer through the wall may be more desirable and should then be used.

(15) The heat absorbed by the liquid may now be estimated:

$$(q_{\text{absorbed by liquid}})_L = h_{tp,L}(T_{w,L} - T_{b,L}) \tag{E6}$$

(16) Compare $q_{absorbed,L}$ by the liquid with the desired q_L and adjust parameters used accordingly and iterate.

REFERENCES

1. Martinelli, R. C., et al.: Isothermal Pressure Drop for Two Phase, Two Component Flow in a Horizontal Pipe. Trans. ASME, vol. 66, no. 2, Feb. 1944, pp. 139-151.

E-976

2. Guerrieri, S. A., and Talty, R. D.: A Study of Heat Transfer to Organic Liquids in Single-Tube Natural-Circulation Vertical-Tube Boilers. Heat Transfer Symposium, Louisville (Ky.), vol. 52, no. 18, 1956, p. 69.

3. Dengler, C. E., and Addoms, J. N.: Heat Transfer Mechanism for Vaporization of Water in a Vertical Tube. Heat Transfer Symposium, Louisville (Ky.), vol. 52, no. 18, 1956, p. 95.

4. Staff of the Lewis Laboratory: Central Automatic Data Processing System. NACA TN 4212, 1958.

5. Woolley, Harold W., Scott, Russell B., and Brickwedde, F. G.: Compilation of Thermal Properties of Hydrogen in Its Various Isotropic and Ortho-Para Modifications. Jour. Res. Nat. Bur. Standards, vol. 41, no. 5, Nov. 1948, pp. 379-475.

6. Johnson, Victor J., ed.: A Compendium of the Properties of Materials at Low Temperature, Phase 1. Cryogenic Eng. Lab., NBS, Dec. 1959.

7. Chelton, Dudley B., and Mann, Douglas B.: Cryogenic Data Book. TR 59-8, WADC, Mar. 1959.

8. Scott, Russell B.: Cryogenic Engineering. D. Van Nostrand Co., Inc., 1959.

9. Farkas, Adalbert: Orthohydrogen, Parahydrogen and Heavy Hydrogen. Cambridge Univ. Press, 1935.

10. McAdams, William H.: Heat Transmission. Third Ed., McGraw-Hill Book Co., Inc., 1954, p. 145.

11. Wolf, H., and McCarthy, J. R.: Heat Transfer to Hydrogen and Helium with Wall to Fluid Temperature Ratios to 11.09. Paper presented at A.I.Ch.E. meeting, Dec. 4-7, 1960.

12. Taylor, Maynard F., and Kirchgessner, Thomas A.: Measurements of Heat Transfer and Friction Coefficients for Helium in a Tube at Surface Temperatures up to 5900° R. NASA TN D-133, 1959.

13. Bernardo, Everett, and Eian, Carrol S.: Heat-Transfer Tests of Aqueous Ethylene Glycol Solutions in an Electrically Heated Tube. NACA WR E-136, 1945. (Supersedes NACA ARR E5F07.)

14. Egen, R. A., Dingee, D. A., and Chastain, J. W.: Vapor Formation and Behavior in Boiling Heat Transfer. Preprint 57A-74, ASME, 1957.

15. Stebbins, J. P.: Effect of Gamma Radiation on the Ortho-Para Conversion of Hydrogen. Rep. ER-10116-23, Martin Co., Aug. 1958.

16. Eley, D. D.: Advances in Catalysis. Vol. 1. Academic Press, Inc., 1948, p. 157.

17. Griffith, R. H., and Marsh, J. D. F.: Contact Catalysis. Oxford Univ. Press, 1957, pp. 79; 114.

18. Robbins, William H., Bachkin, Daniel, and Medeiros, Arthur A.: An Analysis of Nuclear-Rocket Nozzle Cooling. NASA TN D-482, 1960.

TABLE I. - SUMMARY OF HYDROGEN HEAT-TRANSFER DATA FOR 0.375-INCH-OUTSIDE-DIAMETER INCONEL TUBE

[Q = heat flow; q = heat flux; $\dot{W}$ = mass-flow rate.]

Axial distance from tube inlet, L, in.	Local static pressure, p, lb/sq in. abs	Local velocity, u, ft/sec	Average density, ρ_{av}, lb/cu ft	Local quality, x, fraction vapor by mass	Local bulk temperature, T_b, $^\circ R$	Inside wall temperature, $T_{w,i}$, $^\circ R$	Heat-transfer coefficient, h, Btu/sq in.-sec-$^\circ R$
Run 18-2: $\dot{W}$ = 0.177 lb/sec; Q = 2.77 Btu/sec; q = 0.235 Btu/(sq in.)(sec)							
0.055	45.1	82.3	4.02	0	44.5	249.0	0.00115
.64	45.0	87.8	3.77	.004	44.5	192.1	.00159
1.36	44.6	94.9	3.48	.010	44.4	229.6	.00127
2.86	44.0	110.0	3.01	.021	44.3	255.9	.00111
4.36	43.4	125.3	2.64	.032	44.2	266.7	.00101
5.86	42.5	141.3	2.34	.043	44.0	277.6	.00101
7.40	41.5	158.5	2.09	.055	43.9	256.1	.00111
8.44	40.7	170.6	1.94	.062	43.7	252.7	.00112
9.40	39.6	182.8	1.81	.069	43.5	219.9	.00133
10.40	38.7	195.7	1.69	.077	43.3	208.2	.00104
11.40	37.5	209.8	1.58	.084	43.0	166.1	.00191
12.00	36.6	219.1	1.51	.088	42.9	261.0	.00108
Run 18-3: $\dot{W}$ = 0.136 lb/sec; Q = 2.71 Btu/sec; q = 0.230 Btu/(sq in.)(sec)							
0.055	40.6	82.6	3.07	0.018	43.7	249.3	0.00112
.64	40.4	89.4	2.84	.024	43.6	238.0	.00118
1.36	40.1	97.1	2.61	.031	43.6	265.8	.00103
2.86	39.5	113.5	2.23	.046	43.5	266.7	.00103
4.36	38.7	130.6	1.94	.060	43.3	264.0	.00104
5.86	37.8	148.5	1.71	.074	43.1	259.8	.00106
7.40	36.6	168.2	1.51	.089	42.9	230.3	.00122
8.44	35.8	182.1	1.39	.097	42.7	220.4	.00129
9.40	34.4	197.5	1.28	.106	42.4	201.4	.00144
10.40	33.4	213.6	1.19	.115	42.1	173.7	.00174
11.40	31.8	231.9	1.09	.124	41.8	121.3	.00289
12.00	30.7	244.8	1.04	.129	41.5	258.5	.00106
Run 18-4: $\dot{W}$ = 0.093 lb/sec; Q = 2.70 Btu/sec; q = 0.229 Btu/(sq in.)(sec)							
0.055	33.1	65.8	2.63	0.026	42.1	253.6	0.00106
.64	32.9	73.9	2.35	.035	42.0	240.6	.00115
1.36	32.6	83.1	2.09	.045	42.0	263.0	.00104
2.86	31.9	102.8	1.69	.065	41.8	270.4	.00100
4.36	31.3	123.1	1.41	.085	41.6	266.7	.00102
5.86	30.5	144.6	1.20	.105	41.4	264.2	.00103
7.40	29.6	169.0	1.03	.125	41.2	233.2	.00119
8.44	29.0	184.9	.937	.139	41.0	215.6	.00131
9.40	28.0	202.3	.857	.151	40.8	212.2	.00134
10.40	27.4	219.6	.789	.164	40.6	192.5	.00151
11.40	26.4	240.1	.722	.177	40.4	97.2	.00402
12.00	25.7	253.8	.683	.185	40.2	260.5	.00104
Run 18-5: $\dot{W}$ = 0.063 lb/sec; Q = 2.73 Btu/sec; q = 0.231 Btu/(sq in.)(sec)							
0.055	27.3	43.0	2.75	0.020	40.6	259.1	0.00100
.64	27.0	52.5	2.25	.033	40.5	253.3	.00109
1.36	26.8	63.4	1.96	.047	40.5	266.8	.00102
2.86	26.3	88.5	1.36	.076	40.3	271.6	.00100
4.36	25.7	110.7	1.07	.105	40.2	270.4	.00100
5.86	25.2	135.4	.872	.135	40.0	272.6	.00099
7.40	24.6	162.2	.728	.164	39.8	246.8	.00112
8.44	24.1	181.4	.651	.184	39.7	239.2	.00116
9.40	23.4	201.2	.587	.203	39.5	230.7	.00121
10.40	23.0	220.3	.535	.222	39.3	221.8	.00127
11.40	22.2	243.9	.484	.240	39.1	121.1	.00282
12.00	21.7	258.8	.456	.252	38.9	267.2	.00101
Run 18-6: $\dot{W}$ = 0.141 lb/sec; Q = 4.55 Btu/sec; q = 0.385 Btu/(sq in.)(sec)							
0.055	52.2	84.3	4.02	0	44.4	220.0	0.00219
.64	51.9	84.8	4.00	0	44.8	275.2	.00167
1.36	51.6	85.4	3.97	0	45.3	332.6	.00134
2.86	50.9	101.2	3.35	.013	45.5	360.1	.00122
4.36	50.0	123.5	2.75	.031	45.4	363.2	.00121
5.86	49.0	146.5	2.32	.050	45.2	369.2	.00119
7.40	47.6	171.4	1.98	.068	45.0	341.7	.00130
8.44	46.7	188.8	1.80	.081	44.8	332.3	.00134
9.40	45.0	207.0	1.64	.092	44.5	301.1	.00150
10.40	43.8	225.9	1.50	.104	44.3	280.2	.00163
11.40	42.0	247.4	1.37	.115	44.0	191.2	.00262
12.00	40.7	261.8	1.30	.122	43.7	235.6	.00201

TABLE I. - CONTINUED. SUMMARY OF HYDROGEN HEAT-TRANSFER DATA FOR 0.375-INCH-OUTSIDE-DIAMETER INCONEL TUBE

[Q = heat flow; q = heat flux; $\dot{w}$ = mass-flow rate.]

Axial distance from tube inlet, L, in.	Local static pressure, p, lb/sq in. abs	Local velocity, u, ft/sec	Average density, ρ_{av}, lb/cu ft	Local quality, x, % vapor by mass	Local bulk temperature, T_b, ^oR	Inside wall temperature, $T_{w,i}$, ^oR	Heat-transfer coefficient, h, Btu/sq in.-sec-^oR
Run 18-7: $\dot{w}$ = 0.123 lb/sec; Q = 4.61 Btu/sec; q = 0.390 Btu/(sq in.)(sec)							
0.055	45.2	70.5	3.27	0.015	44.6	235.2	0.00205
.64	45.0	81.0	2.84	.026	44.5	358.3	.00124
1.36	44.8	93.0	2.48	.039	44.4	363.3	.00122
2.86	43.9	118.4	1.94	.066	44.3	342.1	.00131
4.36	43.0	144.8	1.59	.093	44.2	327.1	.00138
5.86	41.8	172.8	1.33	.120	43.9	317.7	.00143
7.40	40.4	203.3	1.13	.146	43.6	279.3	.00166
8.44	39.2	225.8	1.02	.164	43.4	275.6	.00168
9.40	37.4	250.5	.920	.180	43.0	273.0	.00170
10.40	36.1	275.6	.836	.197	42.8	258.8	.00181
11.40	34.1	306.5	.752	.213	42.3	158.3	.00336
12.00	32.6	328.9	.701	.223	42.0	237.1	.00200
Run 18-8: $\dot{w}$ = 0.088 lb/sec; Q = 4.63 Btu/sec; q = 0.392 Btu/(sq in.)(sec)							
0.055	37.7	59.4	2.78	0.025	43.1	243.1	0.00196
.64	37.5	71.6	2.31	.041	43.0	357.6	.00125
1.36	37.4	85.4	1.94	.058	43.0	370.3	.00120
2.86	36.6	115.3	1.43	.095	42.9	358.8	.00124
4.36	35.9	146.1	1.13	.132	42.7	351.0	.00127
5.86	34.9	178.8	.925	.168	42.5	346.6	.00129
7.40	33.7	214.8	.770	.205	42.2	313.7	.00144
8.44	32.8	240.9	.686	.230	42.0	306.2	.00148
9.40	31.4	269.4	.614	.252	41.7	291.9	.00157
10.40	30.2	299.7	.552	.275	41.4	276.4	.00166
11.40	28.5	336.4	.492	.297	40.9	190.4	.00262
12.00	27.4	361.2	.458	.311	40.6	242.6	.00194
Run 20-1: $\dot{w}$ = 0.170 lb/sec; Q = 7.05 Btu/sec; q = 0.597 Btu/(sq in.)(sec)							
0.055	57.9	77.1	4.14	0	42.3	218.6	0.00339
.64	57.6	77.8	4.10	0	43.0	452.6	.00146
1.36	57.2	78.7	4.05	0	43.9	526.7	.00124
2.86	56.1	80.6	3.95	0	45.6	533.4	.00122
4.36	54.9	99.7	3.20	.018	46.2	521.0	.00126
5.86	53.5	132.5	2.41	.049	46.0	516.4	.00127
7.40	51.7	168.1	1.90	.080	45.7	473.7	.00140
8.44	50.2	193.7	1.65	.101	45.4	453.1	.00146
9.40	48.1	219.9	1.45	.119	45.1	414.5	.00162
10.40	46.6	247.5	1.29	.139	44.8	391.7	.00172
11.40	44.2	279.6	1.14	.157	44.4	344.1	.00199
12.00	42.4	301.7	1.06	.168	44.0	197.3	.00390
Run 20-2: $\dot{w}$ = 0.136 lb/sec; Q = 7.12 Btu/sec; q = 0.603 Btu/(sq in.)(sec)							
0.055	52.1	61.9	4.11	0	42.8	230.4	0.00322
.64	51.8	62.6	4.06	0	43.7	524.2	.00126
1.36	50.9	63.5	4.00	0	44.8	542.1	.00121
2.86	49.6	87.6	2.90	.026	45.3	505.1	.00131
4.36	48.1	123.9	2.25	.064	45.1	478.4	.00139
5.86	46.5	162.2	1.87	.102	44.8	460.4	.00145
7.40	44.7	204.2	1.25	.140	44.5	421.8	.00160
8.44	43.4	234.4	1.09	.166	44.2	419.2	.00161
9.40	41.6	265.8	.956	.189	43.9	393.8	.00172
10.40	40.3	298.5	.852	.213	43.6	384.5	.00177
11.40	38.4	336.4	.756	.236	43.2	349.3	.00197
12.00	37.1	361.7	.703	.250	43.0	202.3	.00378
Run 20-3: $\dot{w}$ = 0.094 lb/sec; Q = 7.15 Btu/sec; q = 0.606 Btu/(sq in.)(sec)							
0.055	44.0	43.5	4.05	0	43.9	258.1	0.00283
.64	43.6	54.1	3.26	.015	44.3	534.8	.00124
1.36	43.2	73.0	2.41	.041	44.2	530.1	.00125
2.86	42.2	113.6	1.55	.095	44.0	482.8	.00138
4.36	41.1	155.9	1.13	.149	43.8	452.4	.00148
5.86	39.6	201.3	.876	.202	43.5	455.0	.00147
7.40	37.6	253.1	.697	.256	43.1	440.1	.00153
8.44	36.1	291.6	.605	.292	42.8	435.4	.00154
9.40	33.8	335.9	.525	.323	42.2	422.6	.00159
10.40	32.1	381.9	.462	.356	41.8	419.5	.00160
11.40	29.3	444.4	.397	.388	41.1	385.8	.00176
12.00	27.4	490.3	.360	.406	40.6	216.7	.00344

TABLE I. - CONTINUED. SUMMARY OF HYDROGEN HEAT-TRANSFER DATA FOR 0.375-INCH-OUTSIDE-DIAMETER INCONEL TUBE

[Q = heat flow; q = heat flux; $\dot{w}$ = mass-flow rate.]

Axial distance from tube inlet, L, in.	Local static pressure, p, lb/sq in. abs	Local velocity, u, ft/sec	Average density, ρ_{av}, lb/cu ft	Local quality, x, % vapor by mass	Local bulk temperature, T_b, $^{\circ}R$	Inside wall temperature, $T_{w,i}$, $^{\circ}R$	Heat-transfer coefficient, h, Btu/sq in.-sec-$^{\circ}R$
Run 20-4: $\dot{w}$ = 0.079 lb/sec; Q = 7.17 Btu/sec; q = 0.608 Btu/(sq in.)(sec)							
0.055	37.4	42.3	3.48	0.009	43.0	278.2	0.00258
.64	37.0	61.4	2.40	.037	42.9	545.4	.00121
1.36	36.5	83.3	1.77	.067	42.8	545.9	.00121
2.86	35.4	130.9	1.13	.131	42.6	513.0	.00129
4.36	34.0	181.9	.809	.194	42.3	502.7	.00132
5.86	32.5	237.1	.621	.257	41.9	502.7	.00132
7.40	30.7	300.3	.490	.320	41.5	579.1	.00139
8.44	29.4	347.5	.424	.362	41.2	482.2	.00138
9.40	27.6	400.8	.367	.399	40.7	453.3	.00147
10.40	26.2	456.8	.322	.439	40.3	453.8	.00147
11.40	24.1	530.2	.278	.477	39.7	406.4	.00166
12.00	22.7	582.6	.255	.499	39.2	250.5	.00316
Run 22-4: $\dot{w}$ = 0.151 lb/sec; Q = 8.23 Btu/sec; q = 0.697 Btu/(sq in.)(sec)							
0.055	65.0	71.4	3.97	0	45.4	259.4	0.00326
.64	64.7	72.3	3.92	0	46.2	530.6	.00144
1.36	64.4	73.4	3.86	0	47.2	565.9	.00134
2.86	63.4	100.4	2.82	.034	47.5	583.7	.00130
4.36	62.0	134.5	2.11	.076	47.3	563.1	.00135
5.86	60.2	170.7	1.66	.117	47.0	529.6	.00144
7.40	58.0	210.9	1.34	.159	46.7	494.6	.00156
8.44	56.1	239.4	1.18	.186	46.4	480.1	.00161
9.40	54.0	268.3	1.06	.211	46.0	462.2	.00168
10.40	51.4	301.9	.938	.236	45.6	444.8	.00175
11.40	48.1	341.3	.830	.259	45.1	410.6	.00191
12.00	45.8	368.9	.768	.273	44.7	260.2	.00324
Run 20-5: $\dot{w}$ = 0.178 lb/sec; Q = 9.77 Btu/sec; q = 0.828 Btu/(sq in.)(sec)							
0.055	66.4	80.4	4.14	0	42.3	236.0	0.00428
.64	66.1	81.4	4.09	0	43.3	594.2	.00150
1.36	65.6	82.7	4.02	0	44.4	650.0	.00137
2.86	64.6	85.4	3.90	0	46.6	639.2	.00140
4.36	63.4	106.7	3.12	.022	47.5	618.5	.00145
5.86	61.7	147.2	2.26	.064	47.3	601.4	.00150
7.40	59.5	191.8	1.73	.107	46.9	551.7	.00164
8.44	57.7	224.0	1.49	.135	46.6	527.3	.00172
9.40	55.0	257.1	1.29	.160	46.2	479.5	.00191
10.40	52.8	292.8	1.14	.186	45.8	456.6	.00202
11.40	49.4	335.4	.992	.211	45.3	408.2	.00228
12.00	46.7	356.5	.908	.225	44.8	188.5	.00576
Run 20-6: $\dot{w}$ = 0.232 lb/sec; Q = 9.93 Btu/sec; q = 0.841 Btu/(sq in.)(sec)							
0.055	57.9	69.5	4.10	0	43.0	250.2	0.00406
.64	57.6	69.5	4.03	0	44.3	631.0	.00143
1.36	56.9	69.8	3.95	0	45.8	653.2	.00138
2.86	55.7	97.1	2.55	.043	46.3	605.1	.00150
4.36	54.3	143.2	1.73	.099	46.1	566.3	.00162
5.86	52.6	191.7	1.29	.154	45.8	548.1	.00168
7.40	50.1	246.1	1.01	.210	45.4	508.6	.00182
8.44	48.2	286.2	.866	.246	45.1	507.6	.00182
9.40	45.4	330.2	.750	.279	44.6	480.0	.00193
10.40	43.3	376.6	.658	.313	44.2	477.4	.00194
11.40	39.9	436.3	.568	.344	43.5	432.6	.00216
12.00	37.4	480.8	.516	.363	43.0	198.0	.00543
Run 20-7: $\dot{w}$ = 0.093 lb/sec; Q = 9.93 Btu/sec; q = 0.841 Btu/(sq in.)(sec)							
0.055	49.3	42.9	4.05	0	44.0	267.6	0.00376
.64	49.0	49.1	3.53	.009	45.2	653.2	.00138
1.36	48.5	73.0	2.38	.046	45.1	653.7	.00138
2.86	47.4	124.2	1.40	.125	45.0	577.7	.00158
4.36	46.1	177.7	.976	.202	44.7	541.9	.00169
5.86	44.3	235.4	.737	.278	44.4	559.5	.00163
7.40	41.8	301.8	.575	.355	43.9	546.0	.00168
8.44	39.9	351.9	.493	.405	43.5	555.4	.00164
9.40	36.9	411.6	.422	.449	42.9	525.3	.00174
10.40	34.8	473.0	.367	.496	42.5	526.8	.00174
11.40	31.1	562.2	.309	.539	41.6	477.4	.00193
12.00	28.1	638.9	.272	.563	40.8	211.5	.00493

TABLE I. - CONCLUDED. SUMMARY OF HYDROGEN HEAT-TRANSFER DATA FOR 0.375-INCH-OUTSIDE-DIAMETER INCONEL TUBE

[Q = heat flow; q = heat flux; $\dot{W}$ = mass-flow rate.]

Axial distance from tube inlet, L, in.	Local static pressure, p, lb/sq in. abs	Local velocity, u, ft/sec	Average density, ρ_{av}, lb/cu ft	Local quality, x, % vapor by mass	Local bulk temperature, T_b, °R	Inside wall temperature, $T_{w,i}$, °R	Heat-transfer coefficient, h, Btu/sq in.-sec-°R
Run 20-8: $\dot{W}$ = 0.078 lb/sec; Q = 9.89 Btu/sec; q = 0.838 Btu/(sq in.)(sec)							
0.055	41.5	41.7	3.51	0.009	43.9	289.2	0.00342
.64	41.1	65.9	2.22	.048	43.8	679.2	.00132
1.36	40.5	93.7	1.56	.091	43.7	691.3	.00131
2.86	39.2	154.0	.949	.181	43.4	609.0	.00149
4.36	37.7	216.4	.669	.269	43.1	583.1	.00155
5.86	36.1	287.9	.508	.357	42.8	603.8	.00149
7.40	33.9	369.1	.396	.445	42.3	591.4	.00153
8.44	32.2	431.5	.339	.503	41.9	622.4	.00144
9.40	29.8	504.9	.289	.555	41.3	587.8	.00153
10.40	27.9	583.3	.250	.609	40.8	594.5	.00151
11.40	25.3	686.7	.213	.661	40.0	544.2	.00166
12.00	23.2	772.6	.189	.691	39.4	236.7	.00425
Run 22-1: $\dot{W}$ = 0.142 lb/sec; Q = 10.93 Btu/sec; q = 0.926 Btu/(sq in.)(sec)							
0.055	71.1	66.6	3.99	0	45.0	253.7	0.00444
.64	70.7	67.7	3.92	0	46.2	686.0	.00145
1.36	70.2	69.3	3.84	0	47.6	713.7	.00139
2.86	68.7	99.0	2.68	.043	48.3	682.4	.00146
4.36	67.0	141.1	1.88	.104	48.0	647.2	.00154
5.86	64.9	185.9	1.43	.163	47.8	605.2	.00166
7.40	62.2	236.2	1.12	.223	47.4	577.5	.00175
8.44	60.0	273.7	.970	.262	47.0	564.0	.00179
9.40	57.8	311.0	.854	.297	46.7	548.4	.00184
10.40	55.1	352.7	.753	.333	46.2	534.0	.00190
11.40	51.7	401.3	.662	.367	45.7	490.8	.00208
12.00	49.4	434.7	.611	.387	45.3	263.2	.00425
Run 22-2: $\dot{W}$ = 0.101 lb/sec; Q = 10.95 Btu/sec; q = 0.928 Btu/(sq in.)(sec)							
0.055	59.3	47.9	3.96	0	45.5	260.4	0.00432
.64	58.7	52.2	3.64	.006	46.8	688.6	.00145
1.36	58.2	75.1	2.53	.045	46.7	693.3	.00144
2.86	56.7	124.1	1.53	.127	46.5	651.8	.00153
4.36	54.8	175.8	1.08	.207	46.2	619.2	.00162
5.86	52.5	231.5	.820	.286	45.8	609.2	.00165
7.40	49.8	294.2	.645	.365	45.4	604.0	.00166
8.44	47.6	341.5	.556	.417	45.0	597.8	.00168
9.40	45.4	389.6	.487	.464	44.6	586.5	.00171
10.40	42.6	447.8	.424	.511	44.1	575.2	.00175
11.40	39.3	517.7	.367	.556	43.4	519.6	.00195
12.00	37.1	567.3	.335	.582	43.0	266.5	.00415
Run 22-3: $\dot{W}$ = 0.068 lb/sec; Q = 10.94 Btu/sec; q = 0.927 Btu/(sq in.)(sec)							
0.055	48.7	40.0	3.20	0.017	45.2	294.9	0.00371
.64	48.3	63.5	2.01	.067	45.1	741.9	.00133
1.36	47.8	90.4	1.41	.123	45.0	732.3	.00135
2.86	46.5	148.4	.862	.240	44.8	675.2	.00147
4.36	44.9	210.0	.609	.355	44.5	678.0	.00146
5.86	43.0	276.6	.462	.468	44.2	681.2	.00146
7.40	40.6	353.0	.362	.581	43.7	677.6	.00146
8.44	38.7	411.4	.311	.656	43.3	676.4	.00146
9.40	36.6	472.9	.270	.724	42.9	674.7	.00147
10.40	34.3	545.4	.234	.792	42.4	660.2	.00150
11.40	31.5	634.8	.202	.859	41.7	601.7	.00166
12.00	29.6	699.6	.183	.897	41.2	301.5	.00356
Run 20-9: $\dot{W}$ = 0.166 lb/sec; Q = 11.91 Btu/sec; q = 1.01 Btu/(sq in.)(sec)							
0.055	72.3	75.9	4.09	0	43.1	249.6	0.00489
.64	71.9	77.1	4.03	0	44.3	670.7	.00161
1.36	71.3	78.6	3.95	0	45.7	731.9	.00147
2.86	70.1	82.1	3.78	0	48.5	689.4	.00157
4.36	68.5	126.0	2.47	.056	48.3	660.8	.00165
5.86	66.4	172.7	1.80	.112	48.0	641.0	.00170
7.40	63.7	224.7	1.38	.169	47.6	589.5	.00186
8.44	61.6	263.1	1.18	.206	47.3	586.9	.00187
9.40	58.3	305.5	1.02	.238	46.8	513.8	.00216
10.40	55.8	348.3	.892	.272	46.4	496.5	.00224
11.40	51.7	401.7	.773	.305	45.7	436.1	.00258
12.00	46.3	442.7	.702	.321	45.1	190.5	.00694

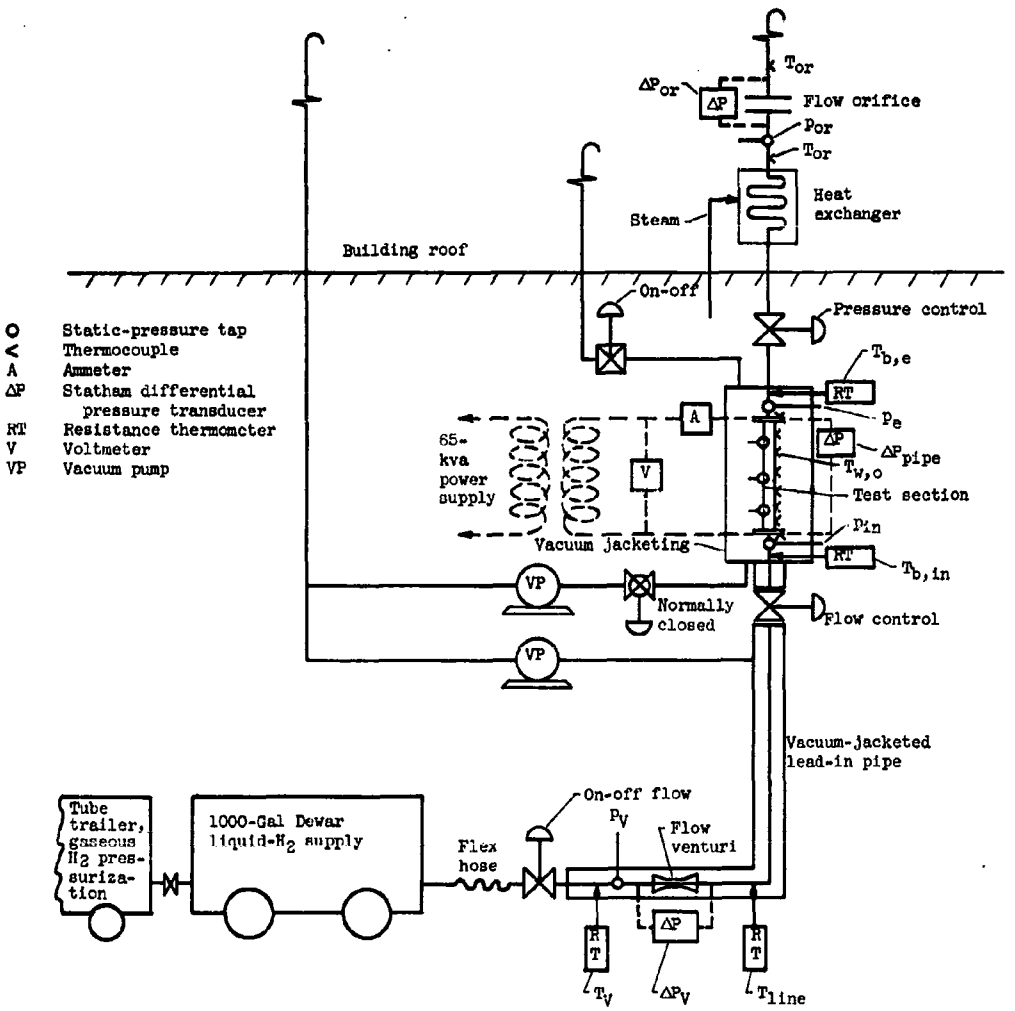

Figure 1. - Schematic diagram of liquid-hydrogen heat-transfer apparatus.

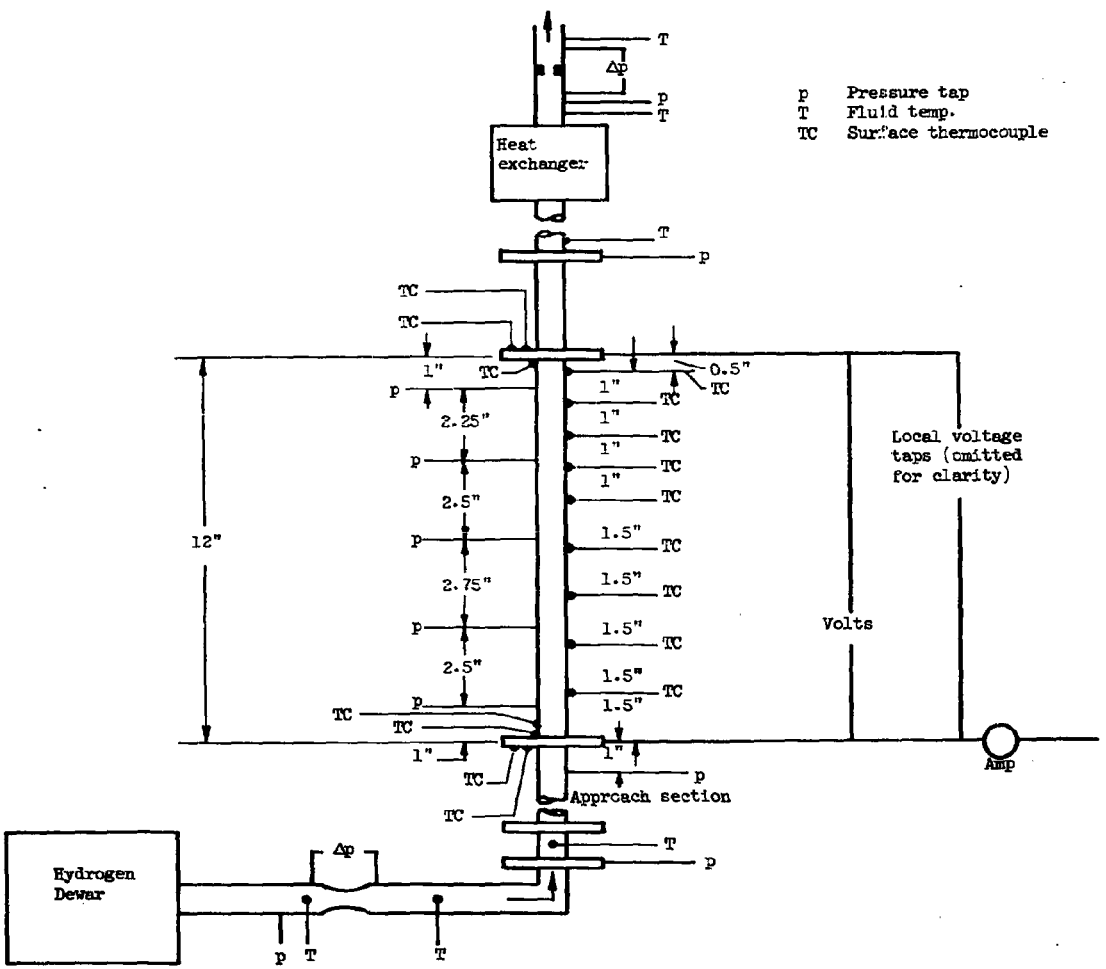

Figure 2. - Schematic of apparatus and instrumentation. (All dimensions are nominal.)

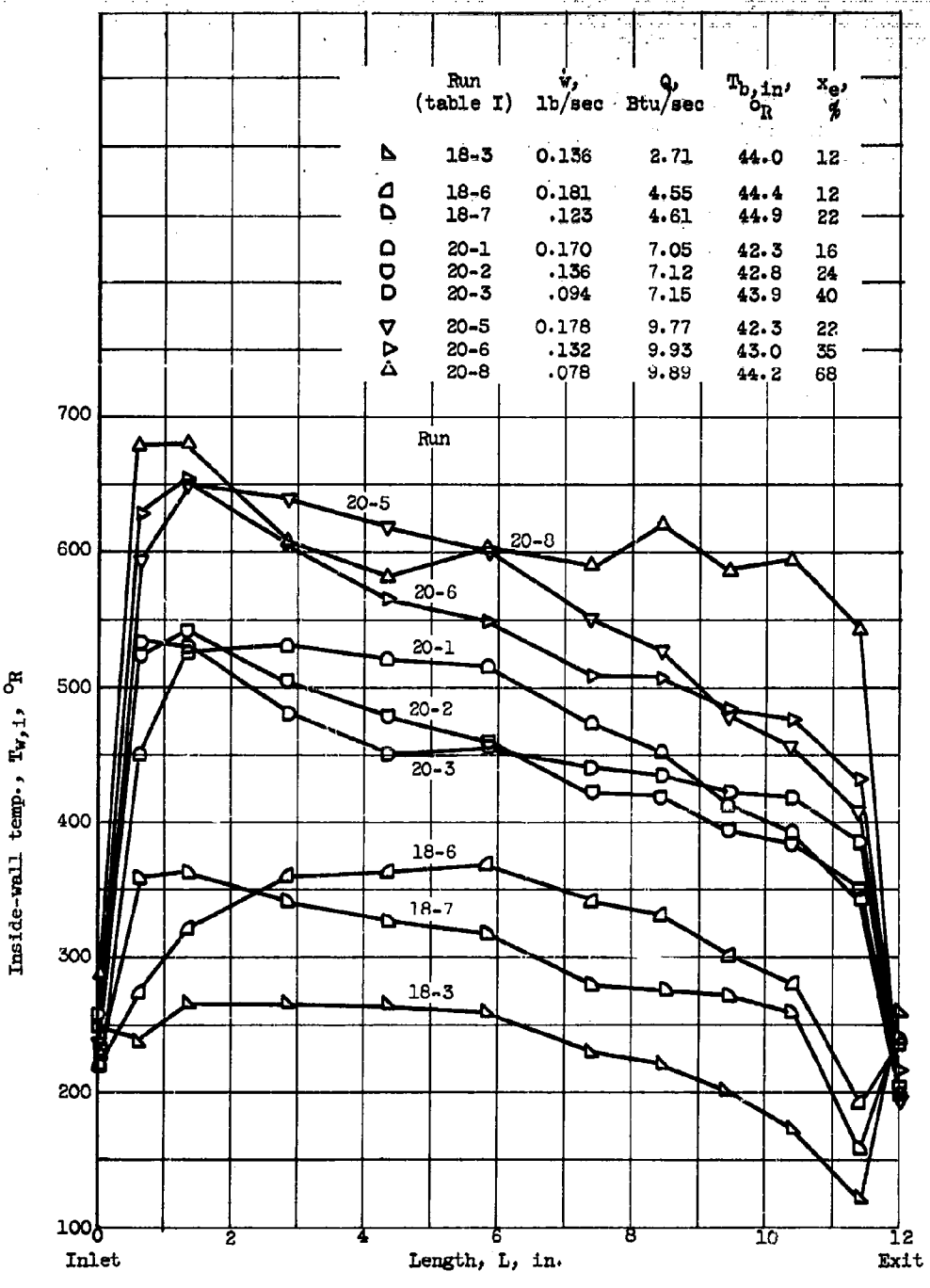

(a) 0.375-Inch-outside-diameter Inconel tube.

Figure 3. - Typical inside-wall temperature distributions.

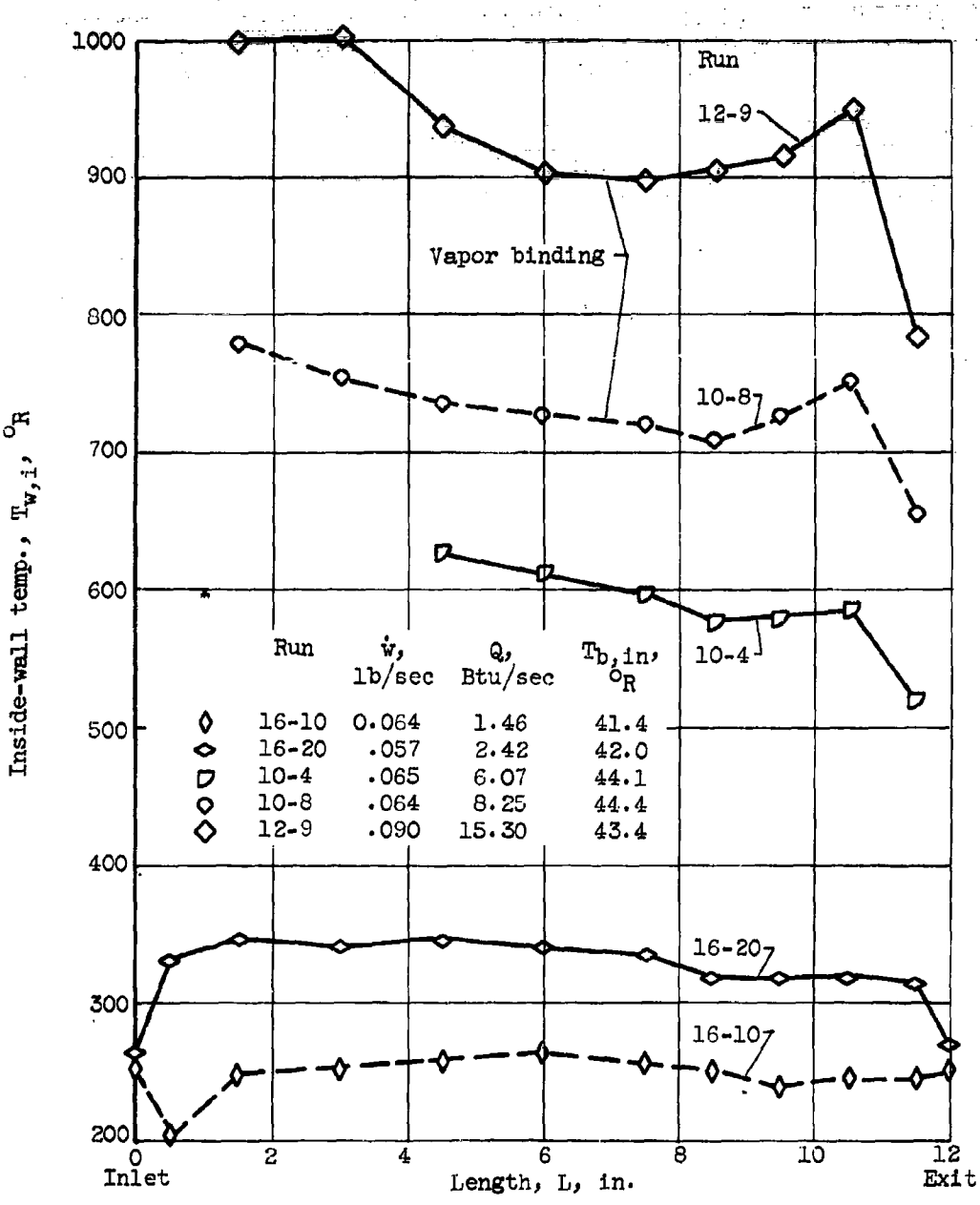

(b) 0.625-Inch-outside-diameter stainless-steel tube. Figure illustrates vapor binding.

Figure 3. - Concluded. Typical inside-wall temperature distributions.

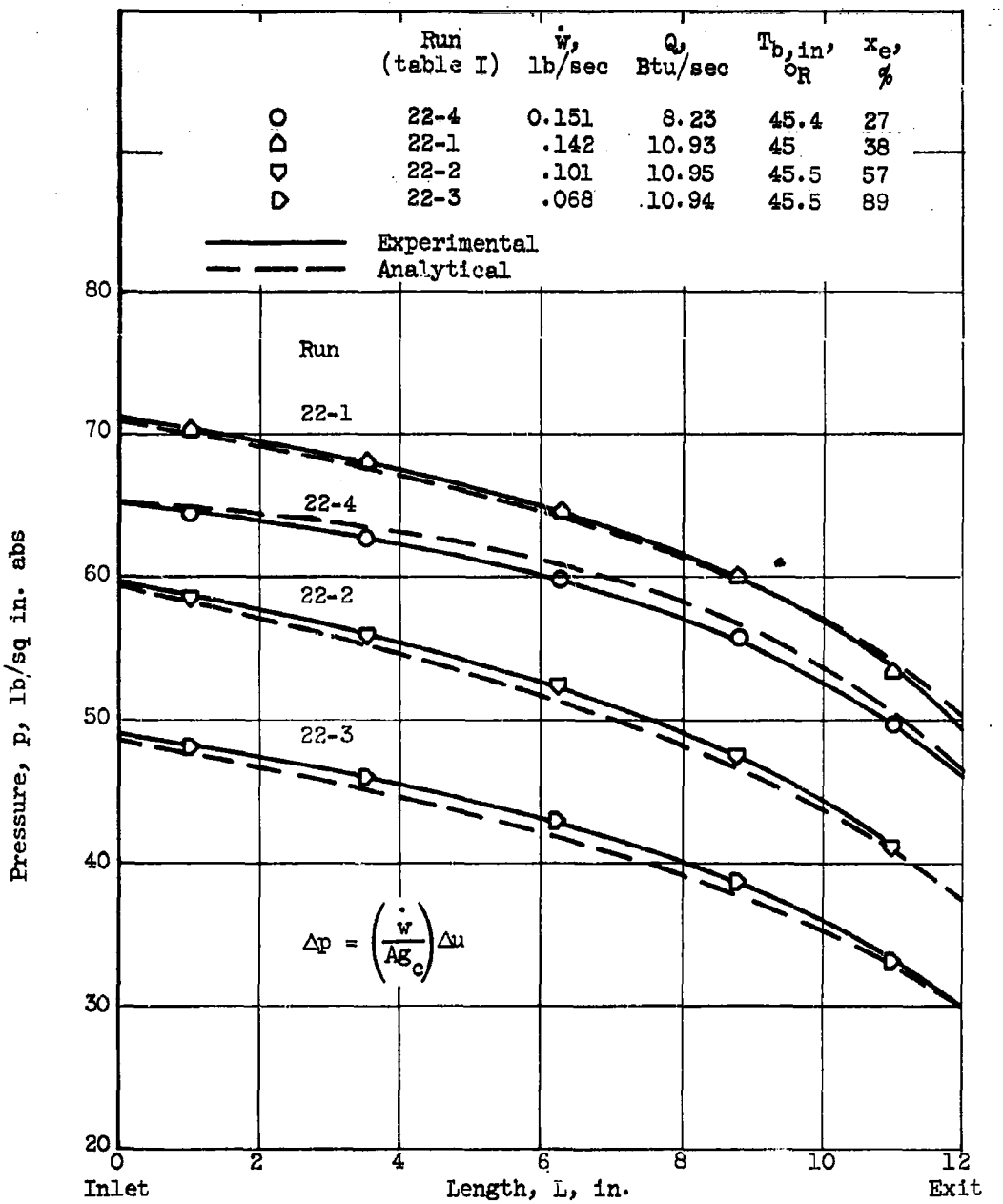

Figure 4. - Comparison of experimental and theoretical pressures along length of test section of 0.375-inch-outside-diameter Inconel tube.

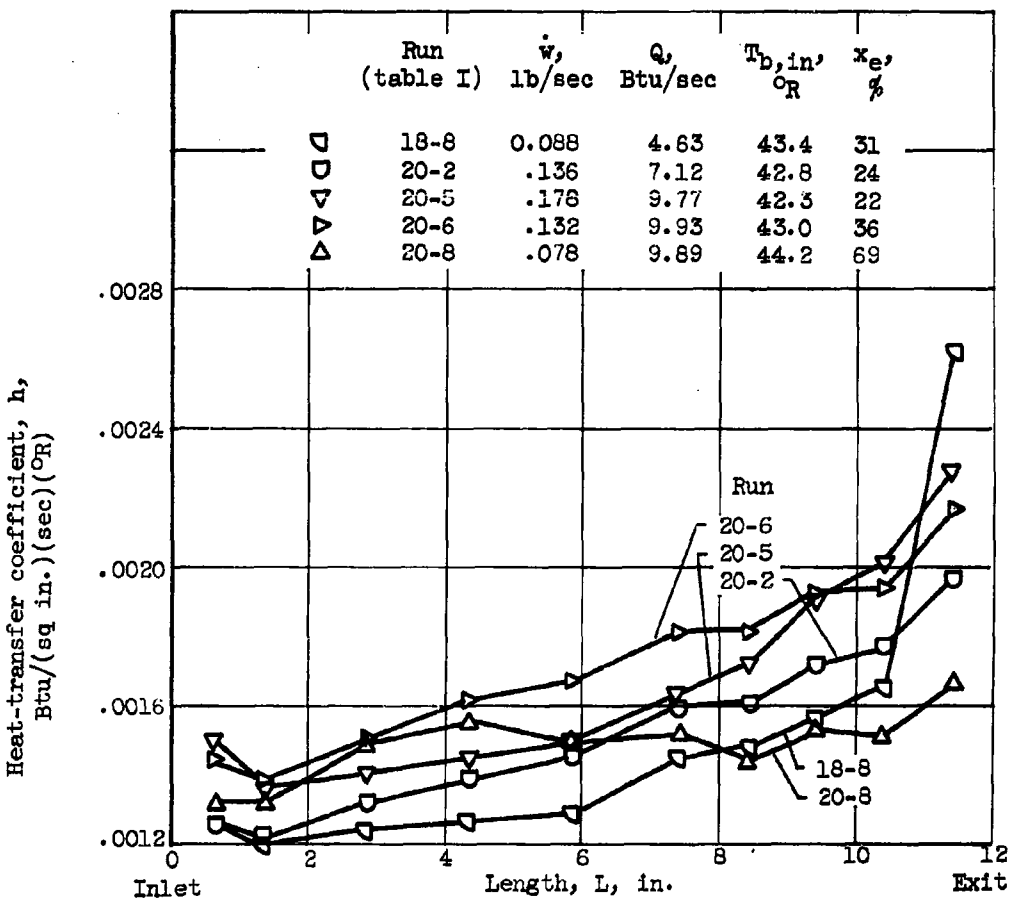

(a) 0.375-Inch-outside-diameter Inconel tube.

Figure 5. - Typical local values of heat-transfer coefficient along length of test section.

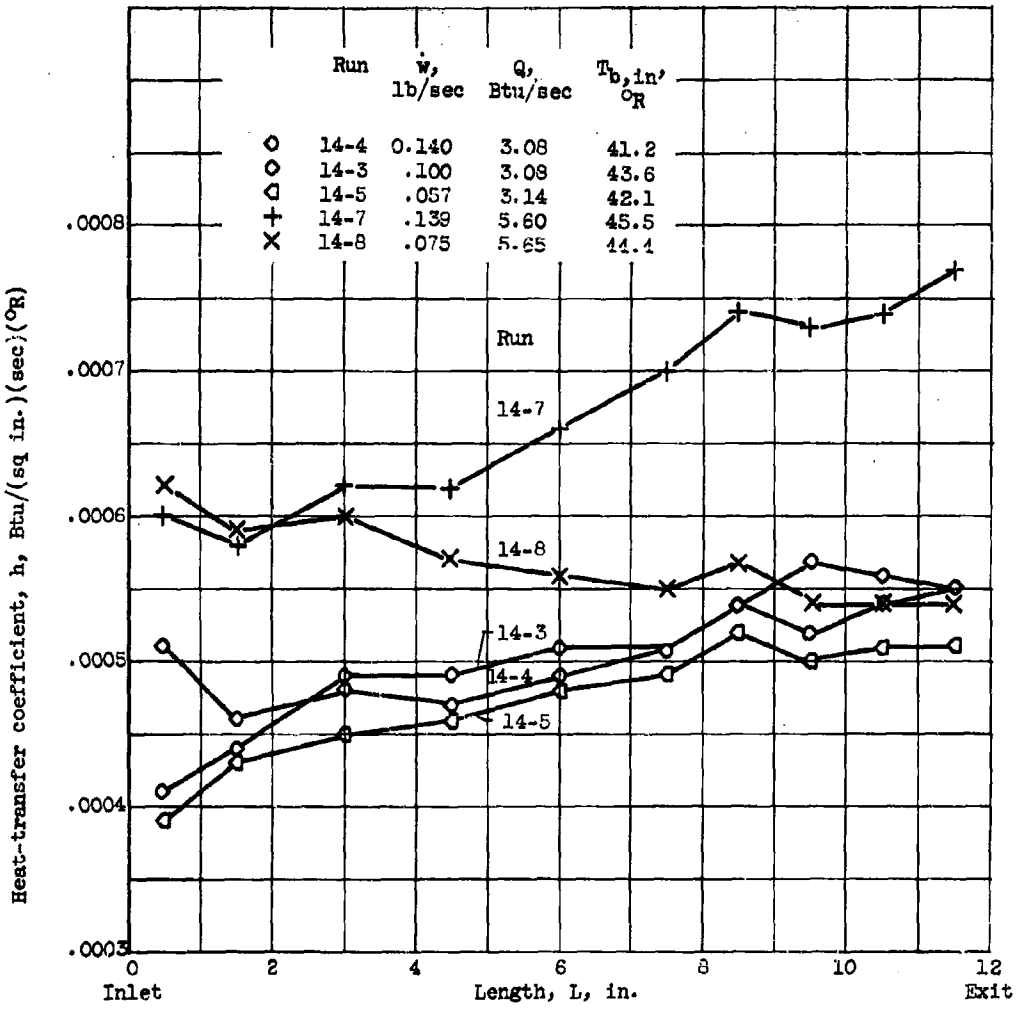

(b) 0.625-Inch-outside-diameter stainless-steel tube.

Figure 5. - Concluded. Typical local values of heat-transfer coefficient along length of test section.

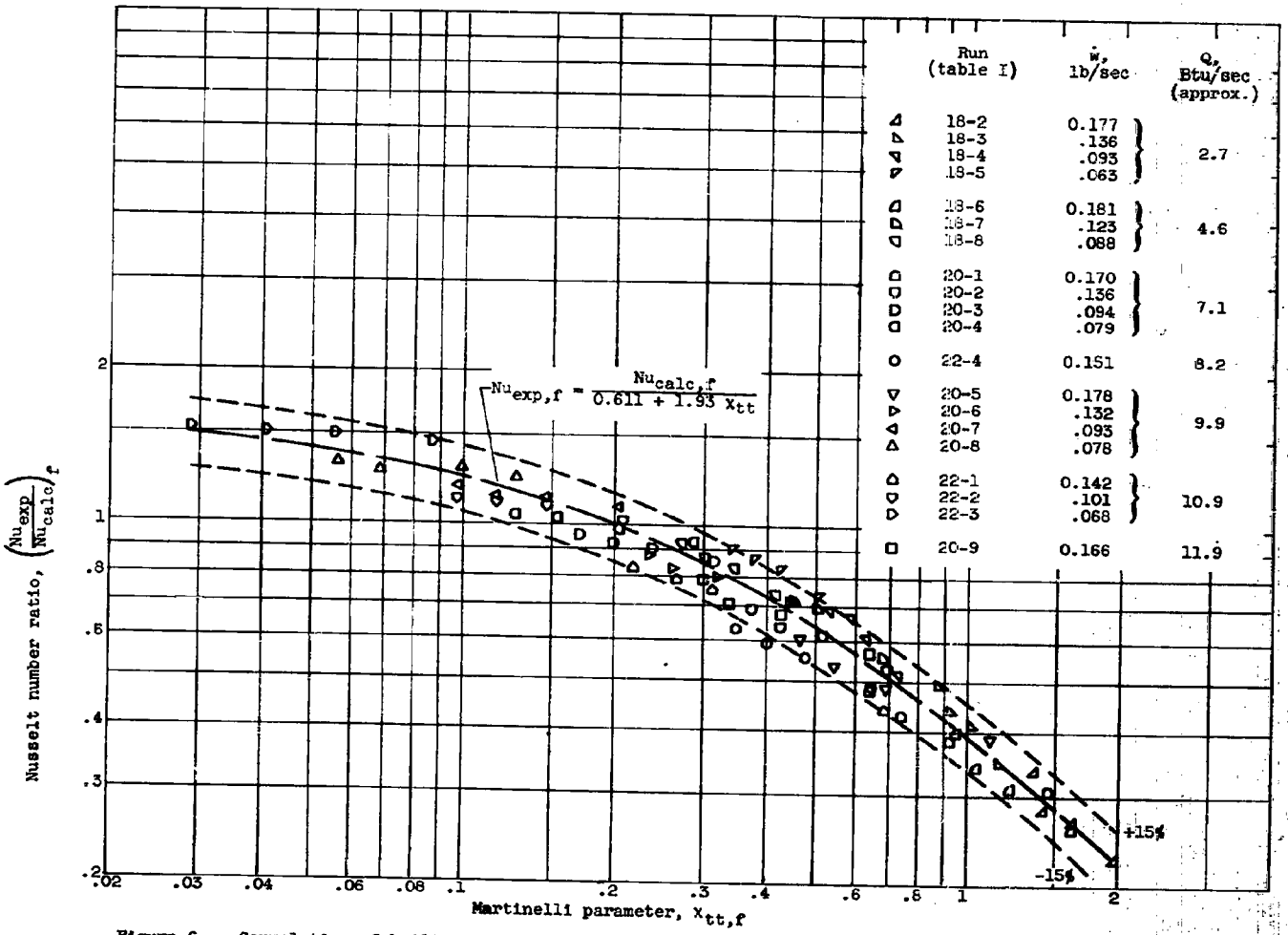

Figure 6. - Correlation of boiling heat-transfer results with Martinelli parameter. Predicted Nusselt number based upon film conditions and corrected for quality; correlation based on data from L = 5.86 to 9.4 inches.

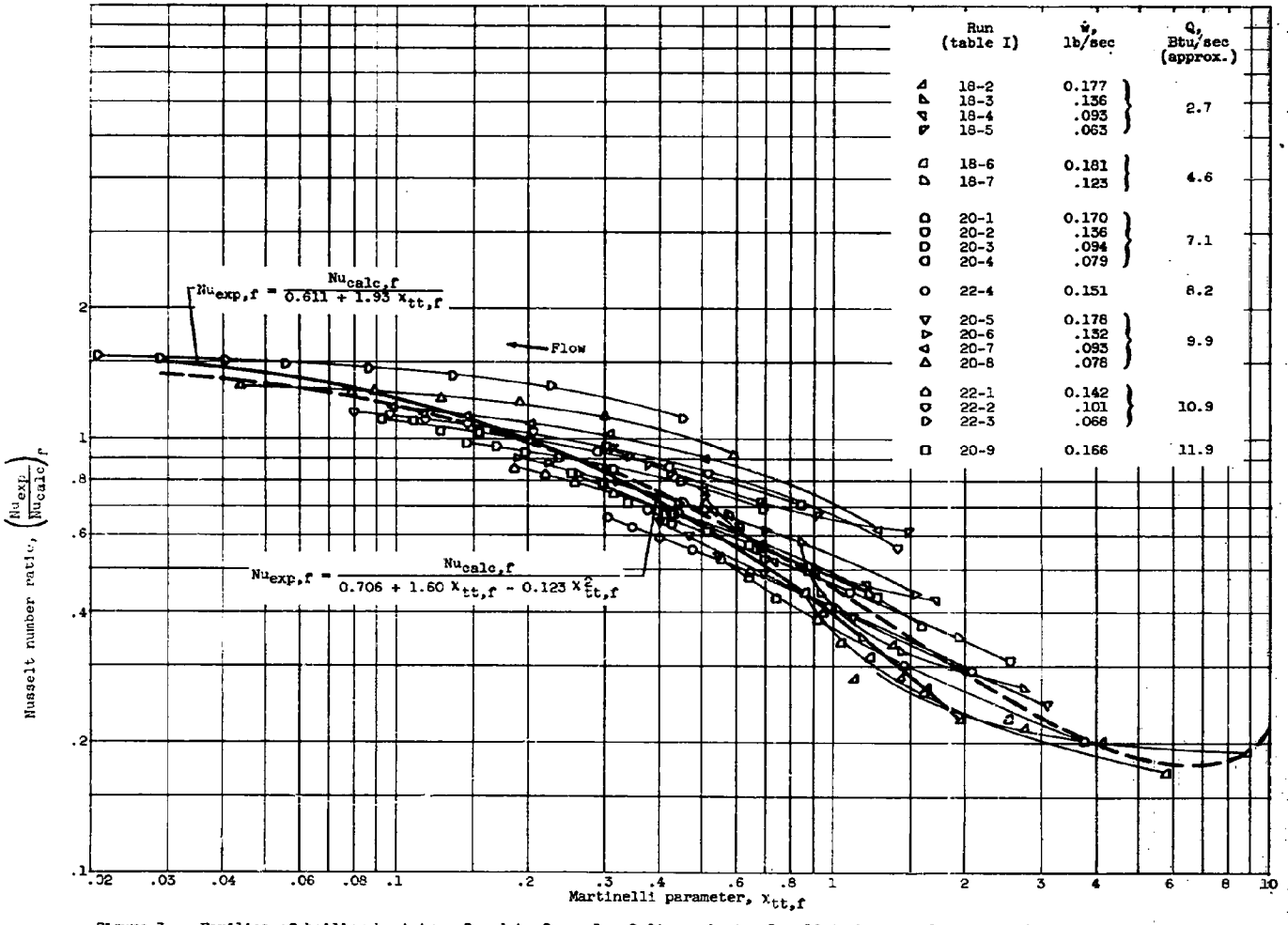

Figure 7. - Families of boiling heat-transfer data from L = 0.64 or >l, to L = 10 inches, as functions of Martinelli parameter and Nusselt number ratio.

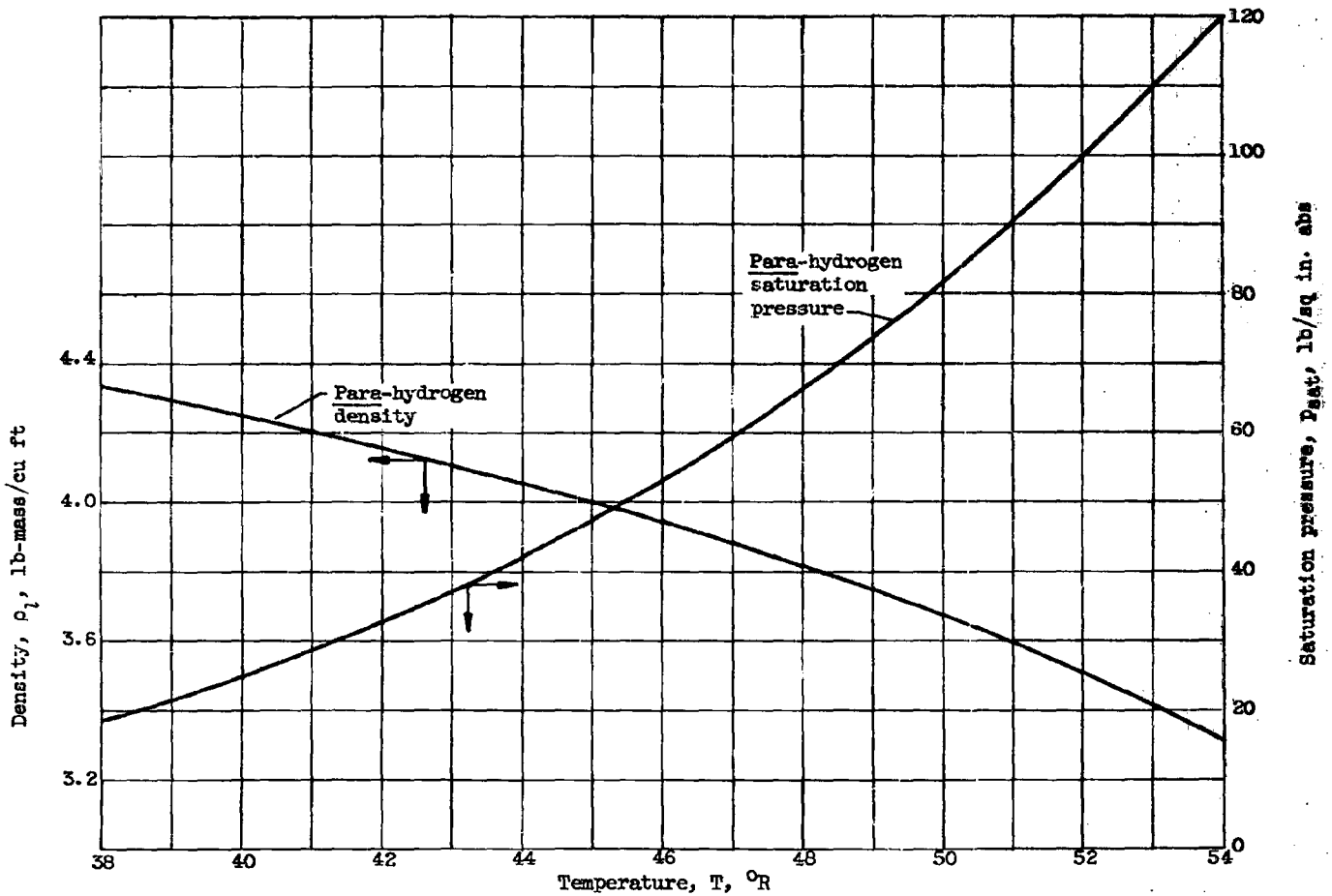

(a) Density and saturation pressure of liquid para-hydrogen (ref. 6).

Figure 8. - Thermodynamic and transport data for liquid and gaseous hydrogen.

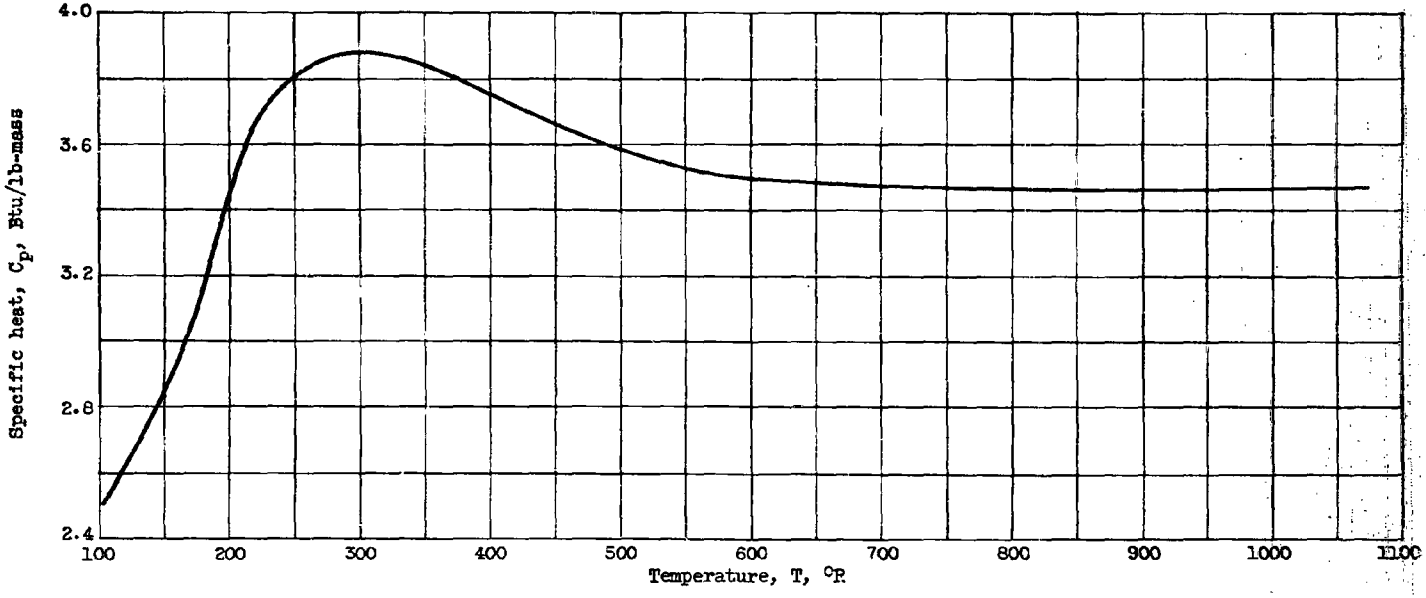

(1) Gaseous hydrogen at 1-atmosphere constant pressure (refs. 5, 6, and 9).

(b) Specific heat.

Figure 8. - Continued. Thermodynamic and transport data for liquid and gaseous hydrogen.

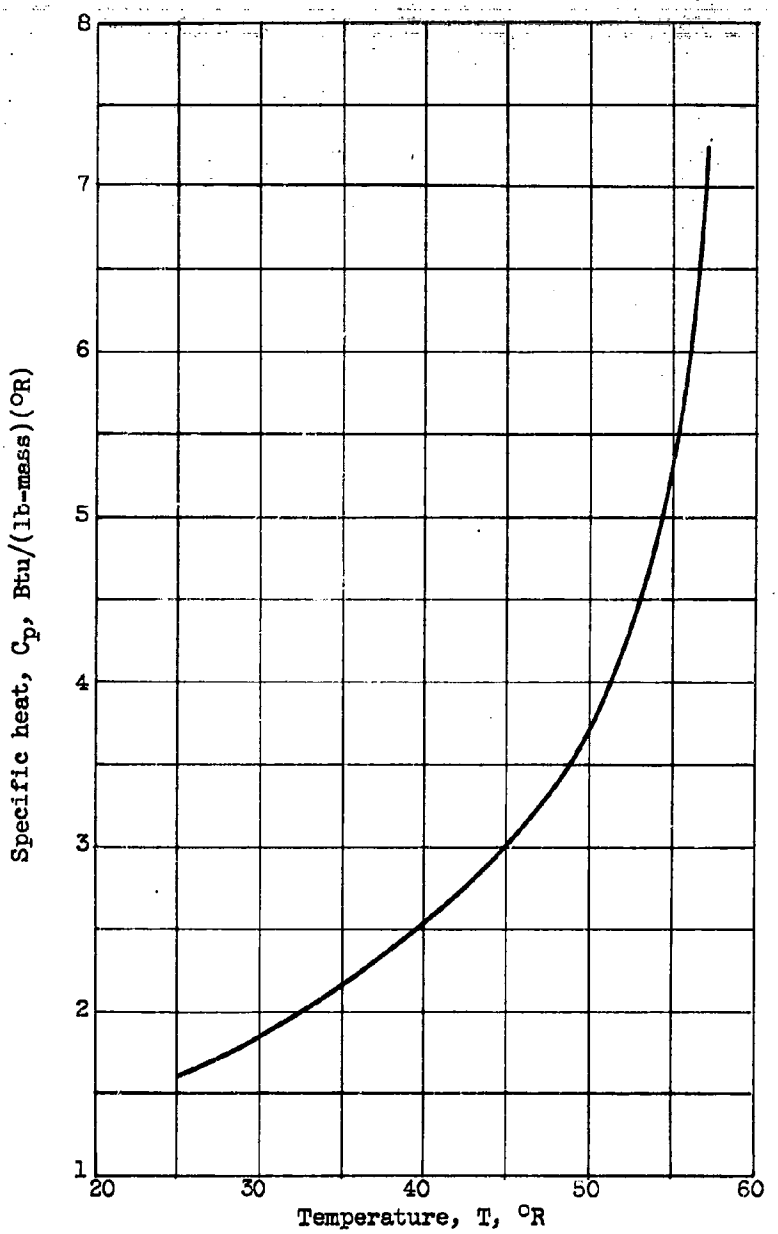

(2) Liquid <u>para</u>-hydrogen (refs. 5 and 6).

(b) Concluded. Specific heat.

Figure 8. - Continued. Thermodynamic and transport data for liquid and gaseous hydrogen.

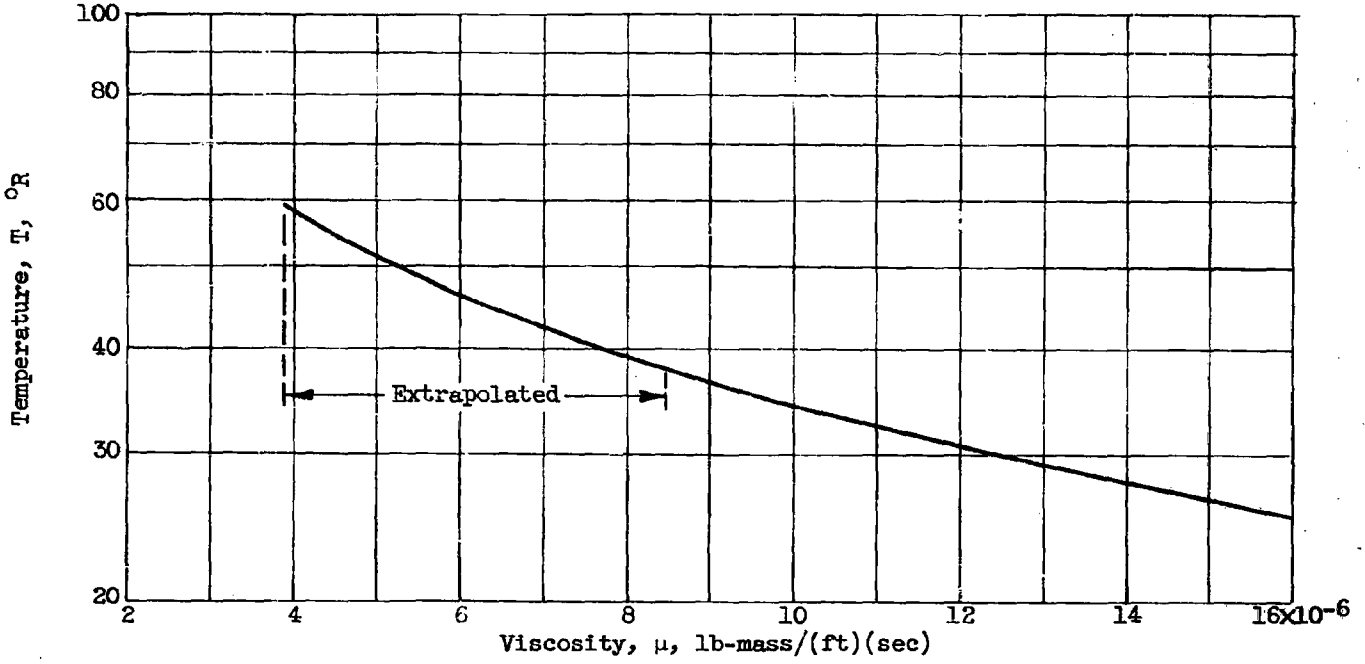

(1) Normal liquid hydrogen (refs. 5 and 6).

(c) Viscosity.

Figure 8. - Continued. Thermodynamic and transport data for liquid and gaseous hydrogen.

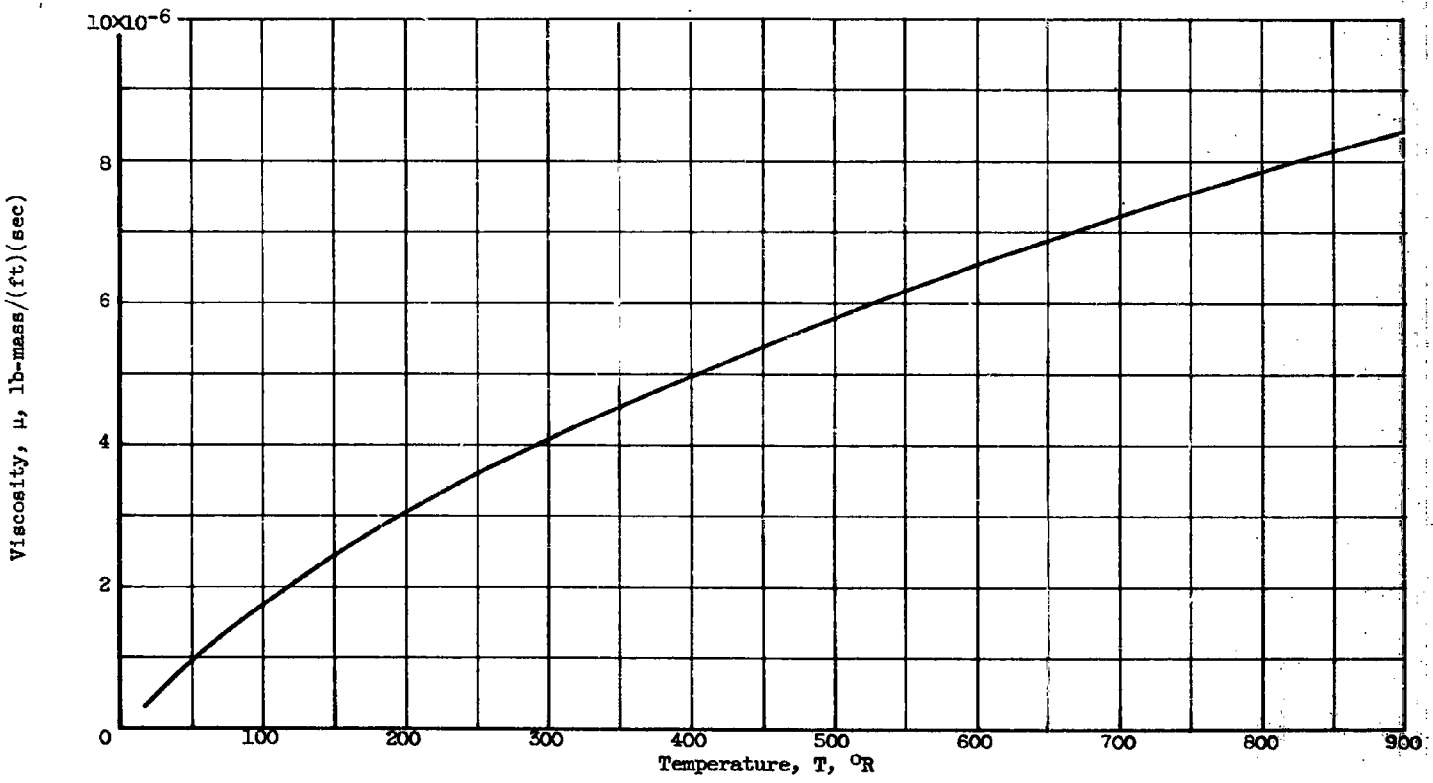

(2) Gaseous hydrogen (refs. 5 and 6).

(c) Concluded. Viscosity.

Figure 8. - Continued. Thermodynamic and transport data for liquid and gaseous hydrogen.

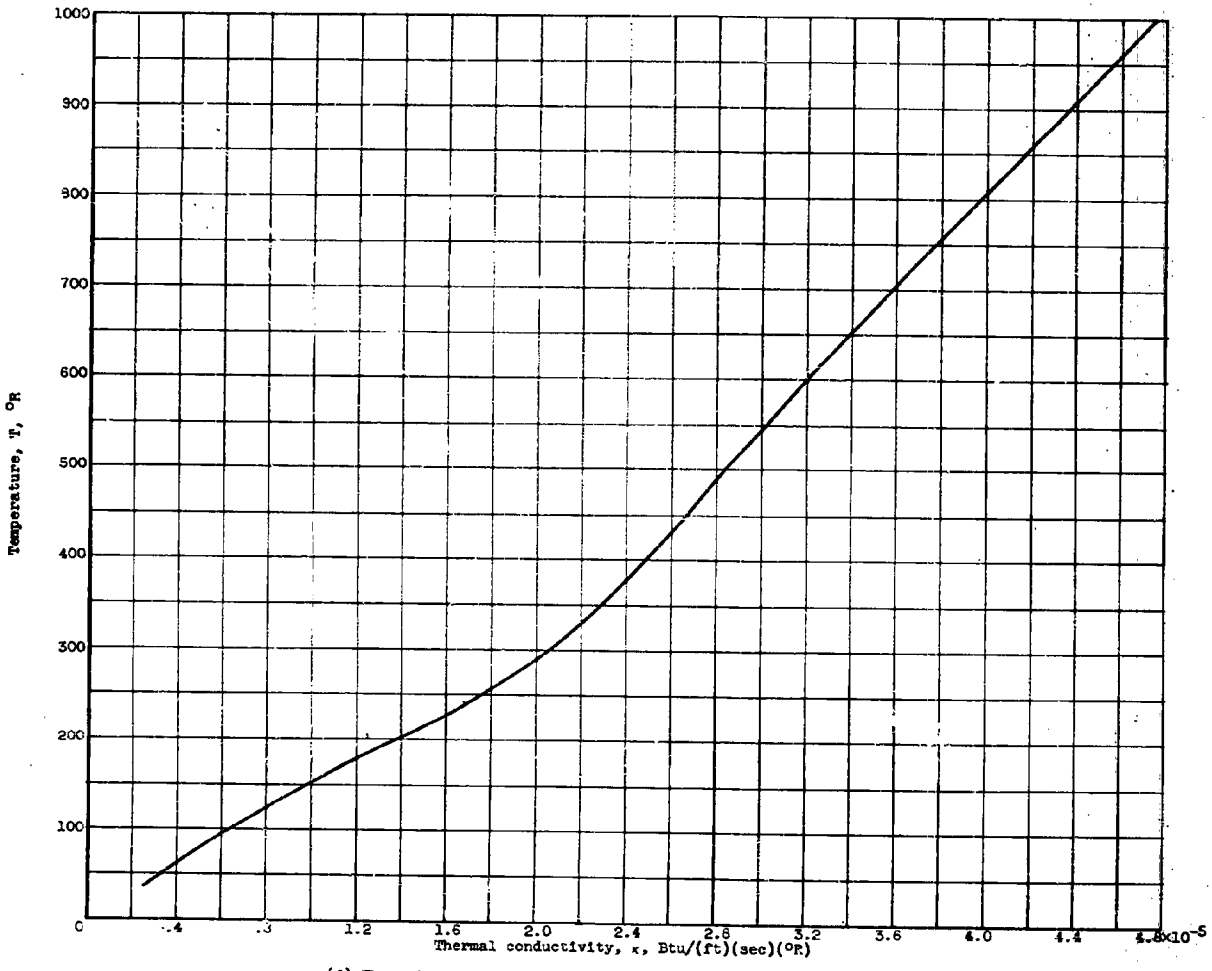

(d) Thermal conductivity of gaseous para-hydrogen (refs. 6 and 9).

Figure 8. - Continued. Thermodynamic and transport data for liquid and gaseous hydrogen.

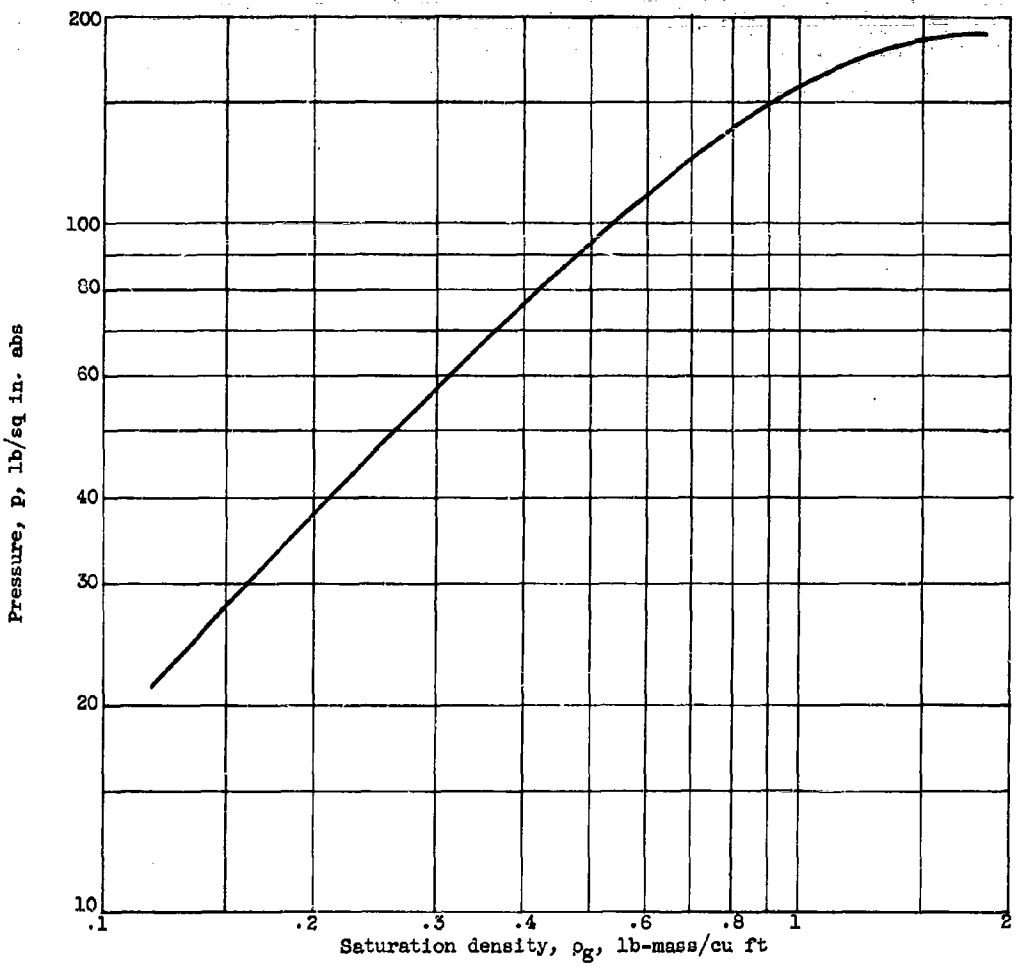

(1) Normal saturated gaseous hydrogen (ref. 5).

(e) Density.

Figure 8. - Continued. Thermodynamic and transport data for liquid and gaseous hydrogen.

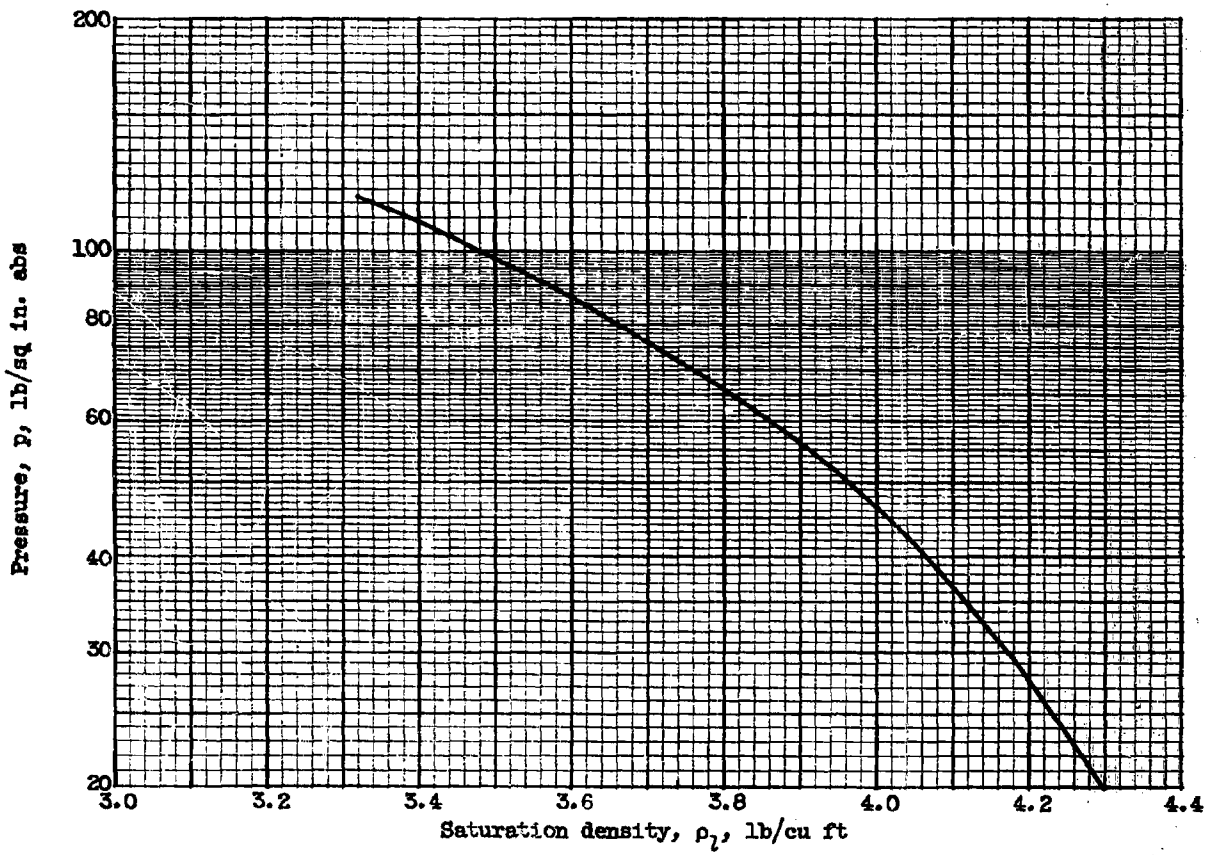

(2) Normal liquid hydrogen (from unpublished data; see also ref. 5).

(e) Continued. Density.

Figure 8. - Continued. Thermodynamic and transport data for liquid and gaseous hydrogen.

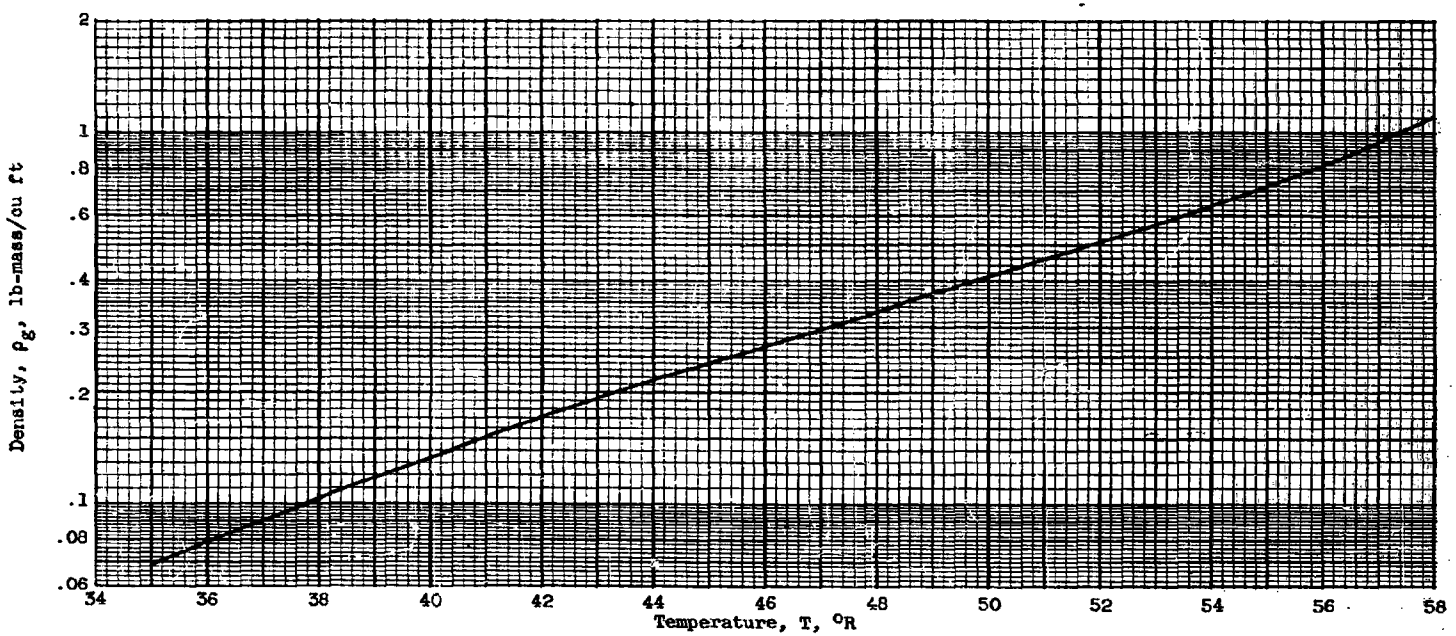

(3) Saturated normal gaseous hydrogen (from unpublished data).

(e) Concluded. Density.

Figure 8. - Continued. Thermodynamic and transport data for liquid and gaseous hydrogen.

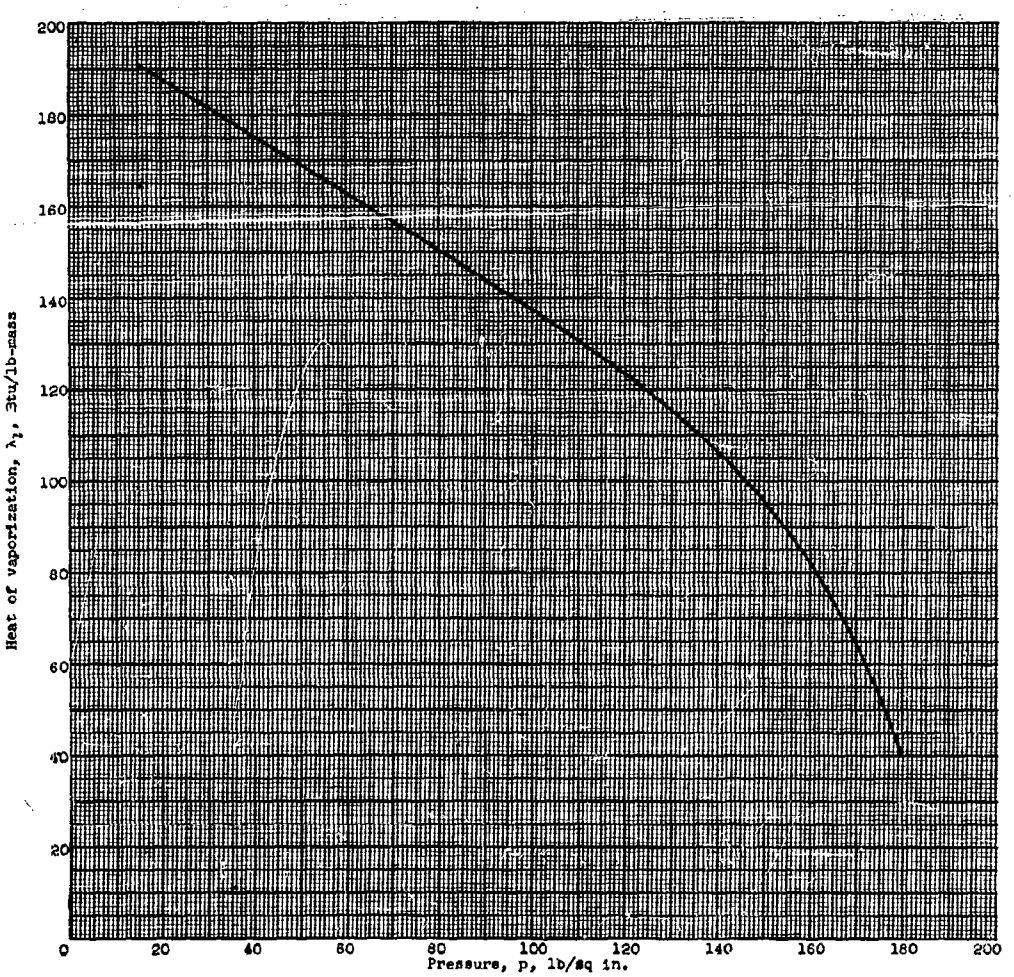

(f) Heat of vaporization of normal liquid hydrogen (from unpublished data; see also refs. 5 and 6).

Figure 8. - Concluded. Thermodynamic and transport data for liquid and gaseous hydrogen.